HYDRODYNAMIC AND EUTROPHICATION MODEL OF THE CHESTER RIVER ESTUARY AND THE EASTERN BAY ESTUARY

DECEMBER 2003 DRAFT REPORT

SUNG-CHAN KIM AND CARL F. CERCO

1 Introduction

Introduction

The Chester River, the Eastern Bay, the Wye River, and the Miles River (Chester system from now on) are tidal water bodies located on the Maryland eastern shore of Chesapeake Bay (Figure 1). The Chester River and the Eastern Bay are connected through a narrow passage. The system has been represented in multiple eutrophication models of the Chesapeake Bay system (Cerco and Cole 1994, Cerco et al. 2002, Cerco and Noel 2003). However, The representation of the river has been coarse in keeping with a grid that represents the entire system. In October 2000, the Environmental Laboratory of the US Army Engineer Research and Development Center (ERDC) entered into an agreement with the Maryland Department of the Environment (MDE) to develop a water quality model of the Chester system. The model was to be used for calculation of Total Maximum Daily Loads for the Chester River and the Eastern Bay Basin. This report is the primary documentation for the model effort.

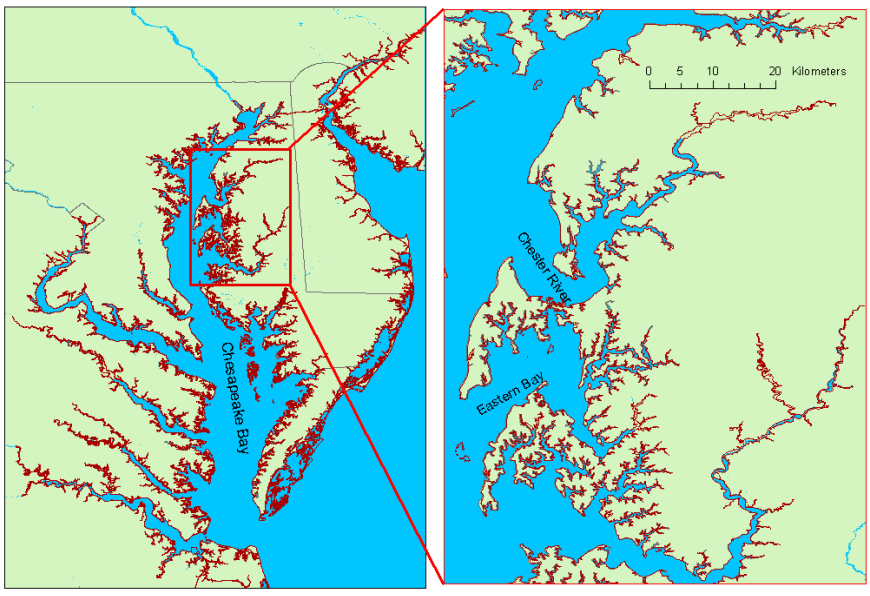

Figure 1. Location Map

Interagency Agreement

Relevant aspects of the agreement to model the Chester system include the followings.

Hydrodynamic Model

Grid. A new grid will be created for this project. The grid will extend from Conowingo dam at the upper end to a location above the Patuxent River entrance at the lower end. The grid will include representations of the Choptank, Chester, and Patapsco Rivers, the Eastern Bay, and other upper bay tributaries. Emphasis will be on fine segmentation in the Chester system and adjacent bay waters. Remaining portions of the system will be more coarsely represented. This grid is intended primarily for examining water quality in the Chester system. Detailed examination of the other tributaries will require regridding with emphasis in the tributary of interest.

Calibration and Application. The hydrodynamic model will be applied to the years 1997-1999. Calibration will be primarily against salinity observations collected by MDE in 1999. Additional calibration will be against NOAA tide observations during the three-year period. Qualitative and quantitative verification against other data sets, including observations in the mainstem bay, will be conducted depending on data availability and resources.

Water Quality Model

The water quality model applied will be the version presently in application to the Bay. This model includes representation of living resources including zooplankton, benthos, and submerged aquatic vegetation. These living resources are not of direct interest in computing TMDLs and modeling them requires extensive data and resources. Consequently, the living resources portion of the model will be left as presently calibrated in the full bay model.

Calibration and Application. The water quality model will be applied to the period 1997-1999. Primary calibration will be against intensive salinity, chlorophyll, nutrient, and dissolved oxygen observations collected by MDE in 1999. Data collected in 1997 and 1998 is sparse. Results from the water quality model will be compared to 1997-1998 data to the extent possible. Model-data comparisons will include observations in the mainstem bay adjacent to the study area.

Loads and Boundary Conditions. The water quality model requires specification of loads at fall lines, from point sources, and from distributed sources. Boundary conditions are required at the open, lower end of the grid. Fall-line and distributed loads in the Chester system will come from a watershed model operated by the MDE. Fall line and

distributed loads in the remainder of the upper bay will come from the EPA watershed model for the entire Chesapeake basin. In the event these loads are unavailable, alternate sources, such as MDE regression models, will be employed. Point source loads throughout the model domain will be provided by MDE. Boundary conditions will come from the EPA monitoring program and data previously provided by MDE from the Choptank River study.

References

Cerco, C., and Cole, T. (1994). "Three-dimensional eutrophication model of Chesapeake Bay," EL-94-4, US Army Corps of Engineers Waterways Experiment Station, Vicksburg MS.

Cerco, C., Johnson, B., and Wang, H. (2002). "Tributary refinements to the Chesapeake Bay model," ERDC TR-02-4, US Army Engineer Research and Development Center, Vicksburg, MS.

Cerco, C., and Noel, M. (2003). "The 2002 Chesapeake Bay eutrophication model," ERDC TR-03-XX, US Army Engineer Research and Development Center, Vicksburg, MS.

2 Hydrology and Loads

Runoff

The major source of freshwater to upper Chesapeake Bay is the Susquehanna River. Flow and associated nutrient loads from this river are strong determinants of conditions outside the Chester system. The Susquehanna is gauged at Conowingo Dam, USGS 01578310 (Figure 1). The year 1997 may be viewed as a dry year (Figure 2). The year 1998 and 1999 exhibited a typical spring peak in March followed by a typical dry summer. There is no available gage in the Chester system. From the EPA watershed model for the whole Bay basin, the above fall-line flows were taken for the system (Figure 3). The flow is, of course, orders of magnitude less than in the Susquehanna. The years 1997 and 1998 had normal spring high flows followed by low summer flows. The year 1999 exhibited relatively low spring flow followed by summer dry period then exhibited a storm peak in September..

Distributed Loads

Distributed loads for the system were obtained from various sources. The primary source for the bay watershed was Phase 4.3 of the US EPA Chesapeake Bay Watershed Model (EPA WSM). The EPA WSM (Linker et al. 2000) is a modified version of the HSPF (Hydrologic Simulation Program FORTRAN) model (Bicknell et al. 1996). Documentation of the latest version of the EPA WSM may be found on the Chesapeake Bay Program web site “http://www.chesapeakebay.net/modsc.htm”. The same model, with more detailed resolution, was applied to the Chester watershed by Maryland Department of the Environment (MDE).

Table 1. Annual Distributed Loads to the Chester Estuary (Chester River and Eastern Bay including Miles, Wye, and Wye East Rivers)

Year	Flow $m^3 s^{-1}$	NH4 kg N d^{-1}	NO3, kg N d^{-1}	Total N kg N d^{-1}	PO4 kg P d^{-1}	Total P kg P d^{-1}	TSS kg d^{-1}
1997	15.45	466	3,948	5,021	231	294	75,591
1998	19.48	533	4,090	5,971	442	574	344,639
*1999	12.07	478	3,041	4,000	270	319	46,458

*1999 includes only the period between January and August.

Software was developed to remove the Chester watershed from the EPA WSM loads and substitute more detailed loads computed by MDE. These were available for all three years 1997-1999. The present calibration is based on distributed flows provided in June 2002 and on loads provided in August 2002. All loads were provided and input to the model on a daily basis. An annual summary of distributed loads to the Chester watershed is provided in Table 1.

The watershed model does not include organic carbon as a state variable. Organic carbon loads at the fall lines in the Chester system watershed were computed as 17.5 times the organic nitrogen load, based on observations at Greensboro at the Choptank River fall line. The ratio 12 was used elsewhere, based on observations at Conowingo.

Point-Source Loads

Twelve municipal and sixteen industrial point-source dischargers are located in the Chester watershed (Figure 4). Loads from these (Table 2 and Table 3) were treated as inputs to the eutrophication model. Monthly flows and concentrations for each discharger were provided by MDE. These were converted into loads and routed to appropriate model locations. No organic carbon concentrations were provided. We computed organic carbon loads as twice the total nitrogen load. This ratio was adapted from the present Chesapeake Bay model (Cerco and Noel 2003). A summary of point-source loads to the estuarine portion of the Chester system is presented in Table 4.

Table 2. Municipal Point-Source Dischargers

NPDES	Facility
MD0020010	Chestertown
MD0020303	Rock Hall
MD0020435	Millington
MD0020559	Sudlersville
MD0020834	Centreville
MD0023370	Queenstown
MD0023485	Kent Island
MD0023604	Talbot County Region II
MD0023876	Eastern Correctional Camp
MD0024384	Chesapeake College
MD0050016	Church Hill
MD0052671	Kennedyville

Table 3. Industrial Point-Source Dischargers		
NPDES	FACILITY	Discharge Points
MD0000345	Kelsicol Chemical Corp.	2
MD0002232	Chestertown Foods, Inc.	6
MD0054933	Sudlersville Frozen Meat	1
MD0000035	S.E.W. Friel	3
MD0000043	S.E.W. Friel - Wye Mills	2
MD0002976	Gordon S. Crouch Seafood	1
MD0065170	U. of MD. Wye Research	1

Table 4. Annual Point-Source Loads to the Chester Estuary (Chester River and Eastern Bay including Miles, Wye, and Wye East Rivers)					
Year	NH4, kg N d^{-1}	NO3, kg N d^{-1}	Total N, kg N d^{-1}	PO4, kg P d^{-1}	Total P, kg P d^{-1}
1997	92	89	228	20	30
1998	66	84	197	18	25
1999	90	43	174	17	24

Bank Loads

Loads from shoreline erosion were adapted from the present Chesapeake Bay model (Cerco and Noel 2003). This load was 3.9 kg d^{-1} silt and fine clay per meter of shoreline. Associated nutrient and carbon concentrations were 0.68 mg g^{-1} phosphorus, 0.33 mg g^{-1} nitrogen, and 4.1 mg g^{-1} organic carbon. Shoreline length of the Chester system is about 455 km, giving total Loads 1.77 x 10^6 kg d^{-1} solids, 1,207 kg d^{-1} phosphorus, 586 kg d^{-1} nitrogen, and 7,275 kg d^{-1} organic carbon.

Wetland Loads

An inventory provided by the EPA Chesapeake Bay Program indicates the Chester system adjoins 31.5 x 10^6 m^2 of emergent wetlands (Figure 5). Based on relationships developed for the present Chesapeake Bay model (Cerco and Noel 2003) wetlands were assigned dissolved oxygen uptake of 2 g m^{-2} d^{-1} and organic carbon export of 0.3 gm^{-2} d^{-1}.

Atmospheric Loads

The EPA Chesapeake Bay Program calculated daily atmospheric nutrient loading to each cell of the system-wide eutrophication model. We converted these loads into equivalent monthly-average areal loads for the Chester estuary (Table 5).

Table 5. Atmospheric Loads to the Chester Estuary

Month	NH4, mg m^{-2} d^{-1}	NO3, mg m^{-2} d^{-1}	Organic N, mg m^{-2} d^{-1}	Organic P, mg m^{-2} d^{-1}
1	0.359	1.425	0.252	0.13
2	0.474	1.396	0.238	0.13
3	0.737	1.62	0.336	0.13
4	0.646	1.272	0.477	0.13
5	0.94	1.535	0.711	0.13
6	0.77	1.255	0.51	0.13
7	0.967	1.484	0.317	0.13
8	0.802	1.33	0.317	0.13
9	0.596	1.157	0.276	0.13
10	0.384	0.954	0.228	0.13
11	0.361	1.078	0.3	0.13
12	0.224	0.95	0.255	0.13

References

Bicknell, B., Imhoff, J., Kittle, J., Donigian, A., Johanson, R., and Barnwell, T. (1996). "Hydrologic simulation program - FORTRAN user's manual for release 11," United States Environmental Protection Agency Environmental Research Laboratory, Athens GA.

Cerco, C., and Noel, M. (2003). "The 2002 Chesapeake Bay eutrophication model," ERDC TR-03-XX, US Army Engineer Research and Development Center, Vicksburg, MS.

Linker, L., Shenk, G., Dennis, R., and Sweeney, J. (2000). "Cross-media models of the Chesapeake Bay watershed and airshed," *Water Quality and Ecosystem Modeling*, 1(1-4), 91-122.

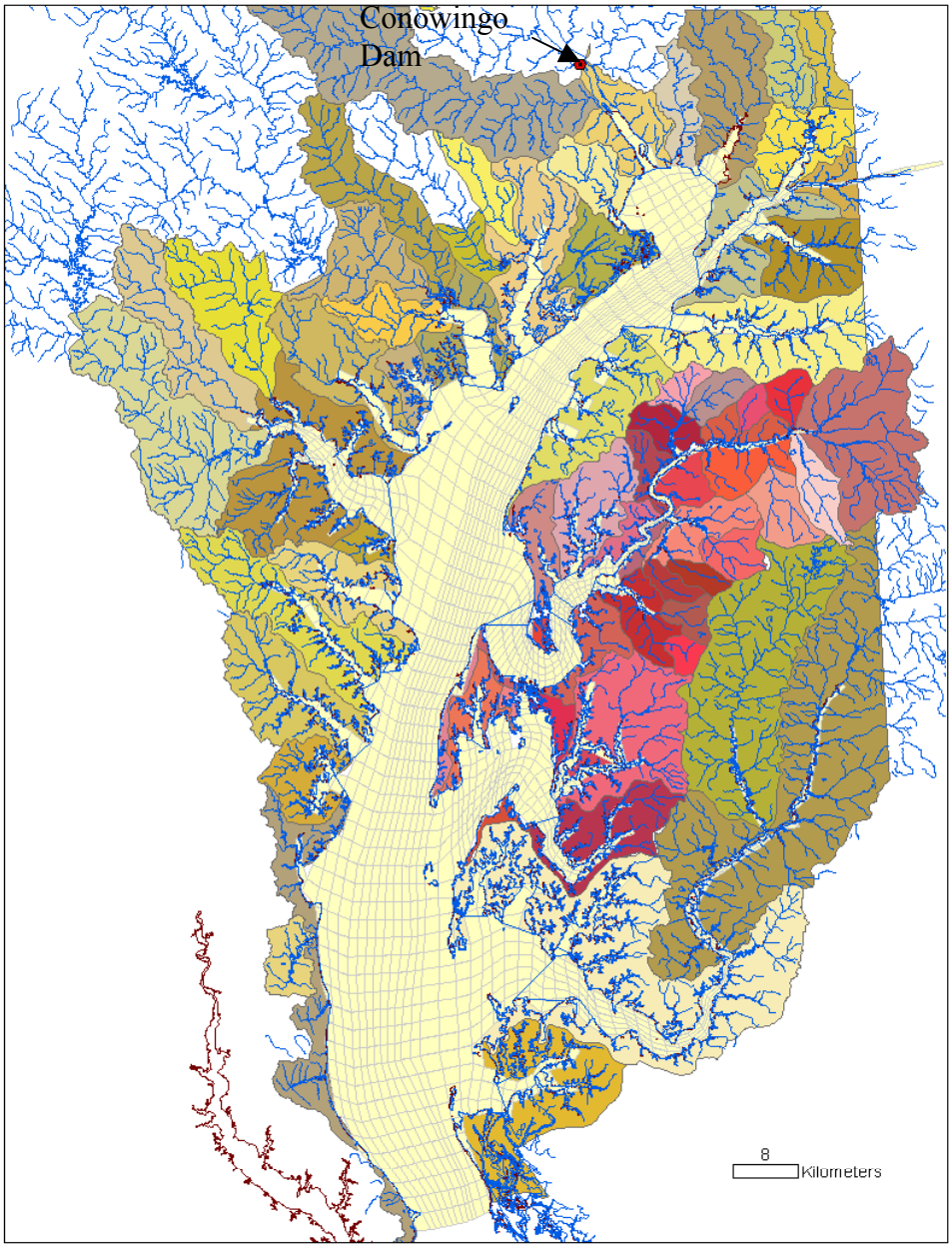

Figure 1. Computational grid overlay with both CBP-HSPF model segments for the Chesapeake Bay basin and MDE-HSPF model segments for the Chester River basin. Also shown is the USGS stream gage 01578310 **at Conowingo Dam in Susquehana River (filled circle).**

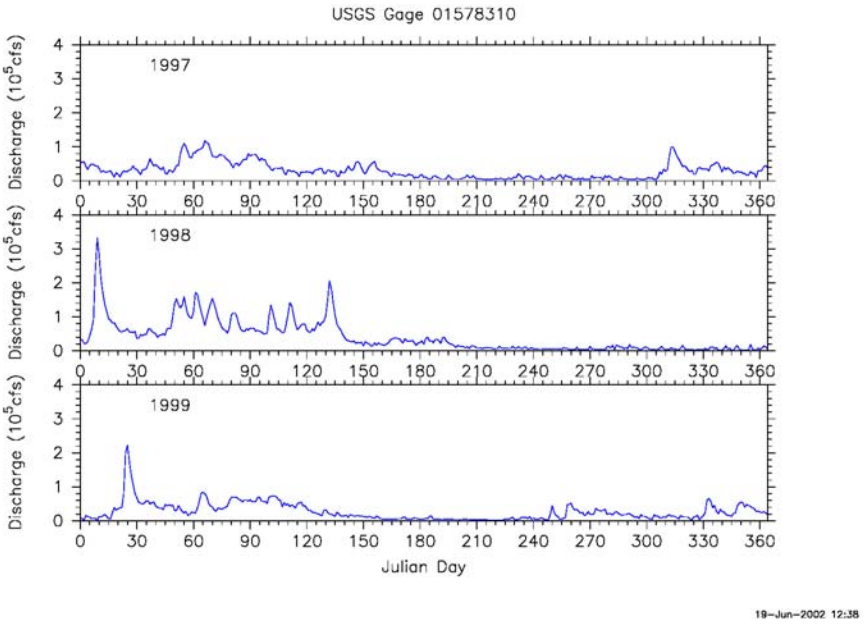

Figure 2. Daily flow in the Susquehanna at Conowingo Dam, 1997-1999

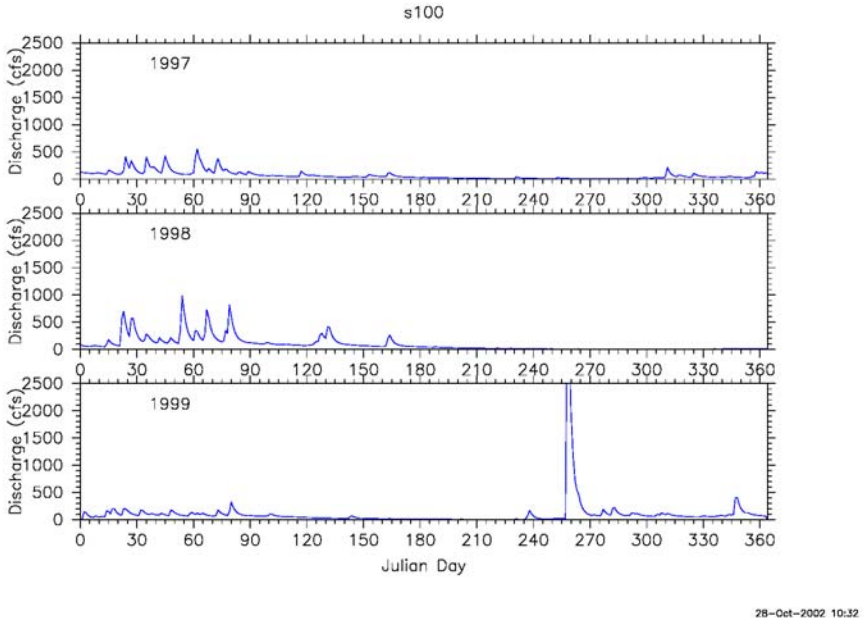

Figure 3. Daily flow in the Chester River driven from watershed model segment S100 at the upstream end, 1997-1999

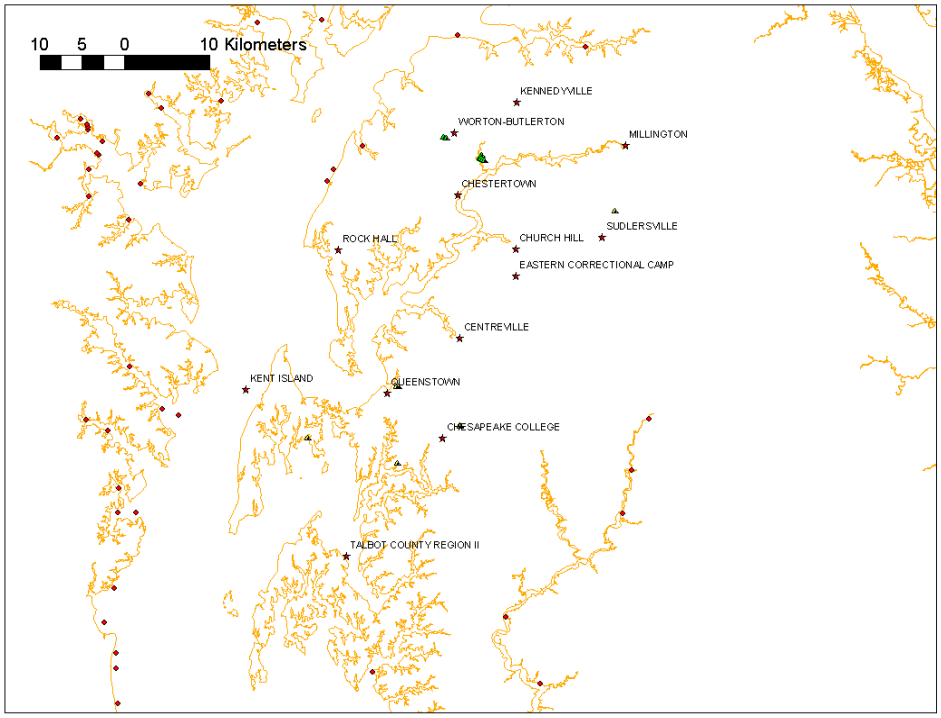

Figure 4. Point source dischargers in the Chester system. Stars represent municipal point sources and triangles represent industrial point sources. Filled circle represents point sources outside the Chester system.

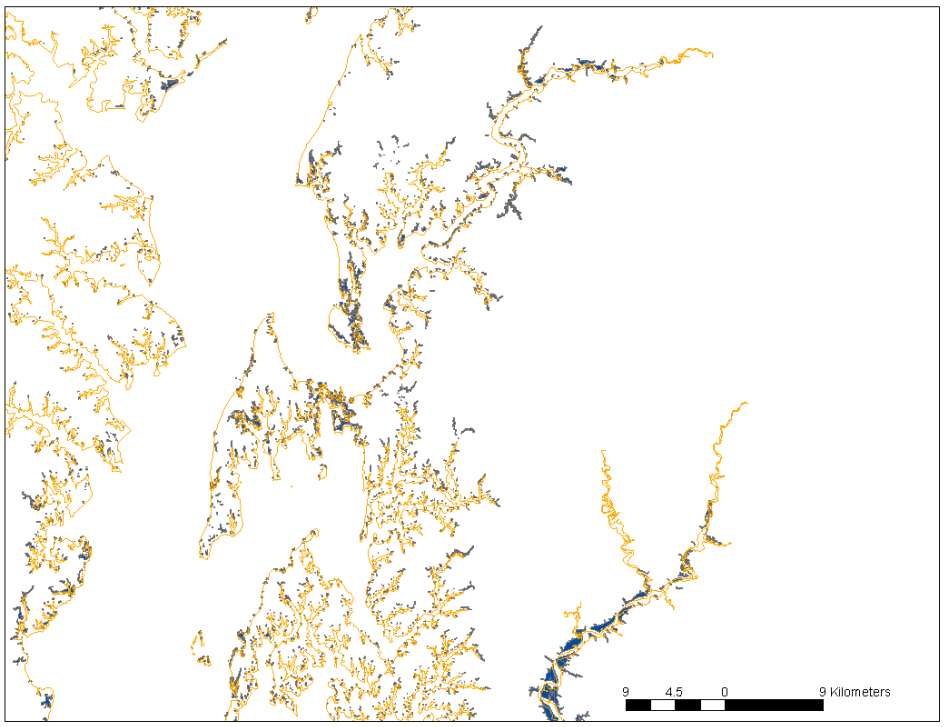

Figure 5. Emergent wetlands in the Chester system.

3 Data Bases

Chesapeake Bay Program

The US Environmental Protection Agency Chesapeake Bay Program conducts regular monitoring of approximately 90 stations in Chesapeake Bay and tributaries. Observations have been collected 10 to 20 times per year since mid-1984. Observations collected in upper Chesapeake Bay and in the Chester system (Figure 1) formed the basis for temporal calibration and verification of the model over the three-year interval 1997-1999. These observations were downloaded from the Chesapeake Bay Program web site. Stations of particular interest in the Chester system were ET4.1, ET4.2, and EE1.1.

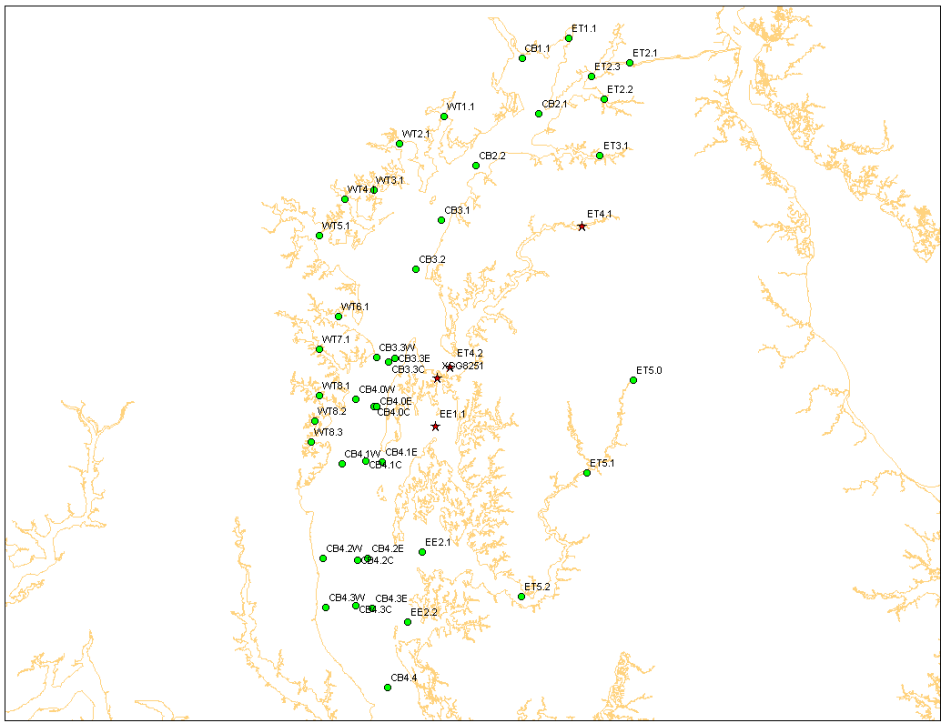

Figure 1. Chesapeake Bay Program long term monitoring stations. Stations in the Chester system, ET4.1, ET4.2, EE1.1, and XGG8251, were marked as stars. Rest of the stations are represented by filled circles.

Circa mid-1998, analytical laboratories and methods were changed in the Chester stations. Analyses of total Kjeldahl nitrogen and total phosphorus were discontinued. Analyses of total dissolved nitrogen, particulate nitrogen, total dissolved phosphorus, and particulate phosphorus were initiated. Direct analysis of particulate carbon was substituted for derivation of particulate carbon by difference. The change in analytical techniques caused the appearance of step-change differences in organic nitrogen, phosphorus, and carbon parameters.

Maryland Department of Environment

Maryland Department of Environment conducted six surveys on the Chester system in 1999, three in spring and three in summer. Spatial coverage was extensive (Figure 2). A total of sixty-one stations in the estuarine portion were sampled. These surveys provided the basis for spatial calibration and verification of the model.

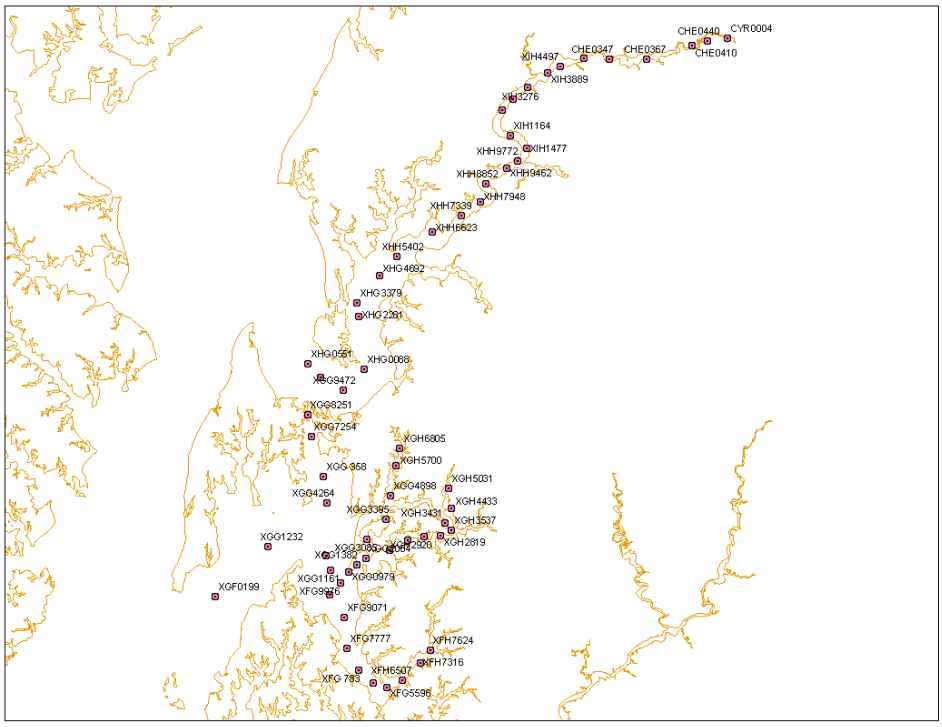

Figure 2. MDE intensive survey stations of the estuarine portion in the Chester system.

Sediment Oxygen and Nutrient Exchange

Measures of sediment oxygen and nutrient exchange were available during summer period of 2000 at 20 stations in the Chester River (Figure 3).

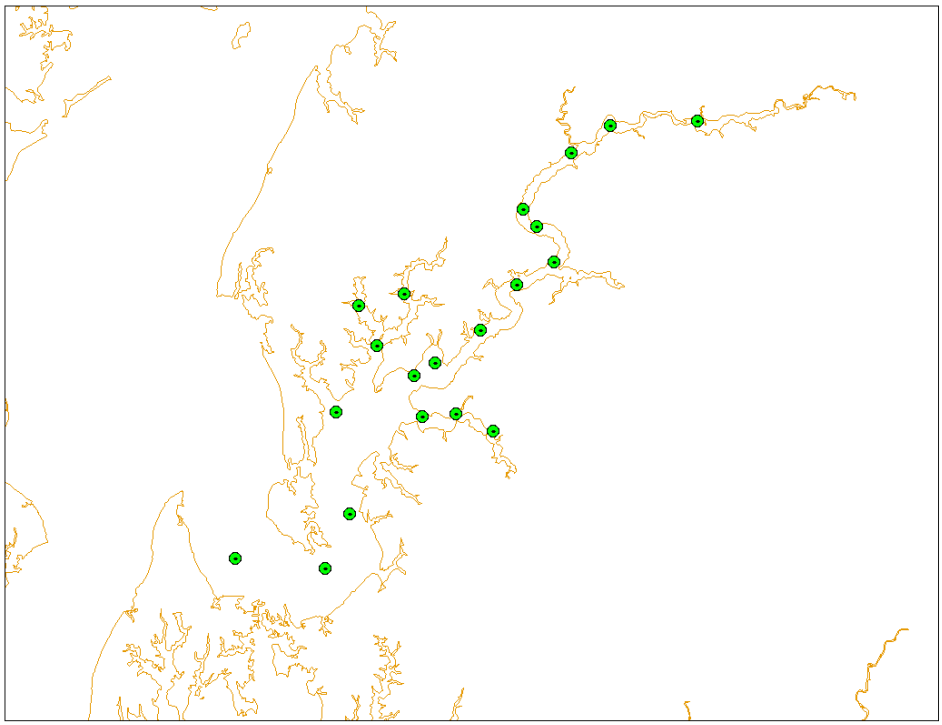

Figure 3. Benthic flux monitoring stations in the Chester River.

4 The Hydrodynamic Model

The Numerical Model

Theoretical Aspects

The CH3D-WES (Computational Hydrodynamics in Three Dimensions - Waterways Experiment Station) model makes computations on a generalized curvilinear or boundary-fitted horizontal grid. However, to ensure that long-term stratification in the deep channels is maintained, the vertical grid is Cartesian. Boundary-fitted grids in the horizontal directions allow for a better representation of the bay's boundary as well as internal features such as channels and islands.

All physics impacting circulation and mixing in water bodies such as Chesapeake Bay are included. These include the impact of freshwater inflows, tides, wind forcing, the impact of the earth's rotation, surface heat exchange, and the effect of turbulence on the mean circulation. The vertical turbulence closure model computes the eddy viscosity and diffusivity from the kinetic energy and dissipation of the turbulence. This type of closure model is known as a k-ε turbulence model. The production of turbulence occurs due to wind stress at the surface, velocity shear in the water column, and bottom friction. Density effects due to salinity and temperature are fully coupled with the developing flow field. Thus, advection/diffusion equations for the salinity and temperature are solved along with the conservation of mass and momentum equations for the flow field. An equation of state relates the water density to the salinity and temperature fields. Surface heat exchange is modeled through the Edinger et al.'s (1974) concept of an equilibrium temperature.

The numerical algorithm consists of an external and an internal mode. The two-dimensional (2D) water surface field and vertically-averaged velocities are computed in the external mode, with the water surface elevations then employed in the computation of the horizontal pressure gradient in the internal mode. Terms such as the vertically-averaged advection in the external mode are computed by summing up the 3D computations over the water column. The 3D velocities, salinity, and temperature are computed in the internal mode. The 3D velocities are adjusted to ensure that water flux over the water column is consistent between the external and internal modes. The computational scheme is such that the speed of a free-surface gravity wave is removed from the stability criteria controlling the size of the computational time step. However,

other criteria remain (e.g., the advective speed of the water). Model details can be found in Sheng (1986) and Johnson et al. (1991, 1993).

Model Grid

The numerical grid for the Chester system is shown in Figure 1. As can be seen, the modeled domain extends from the Susquehanna River southward to a location just above the Patuxent River entrance. All major tributaries and embayments along eastern and western shores are included.

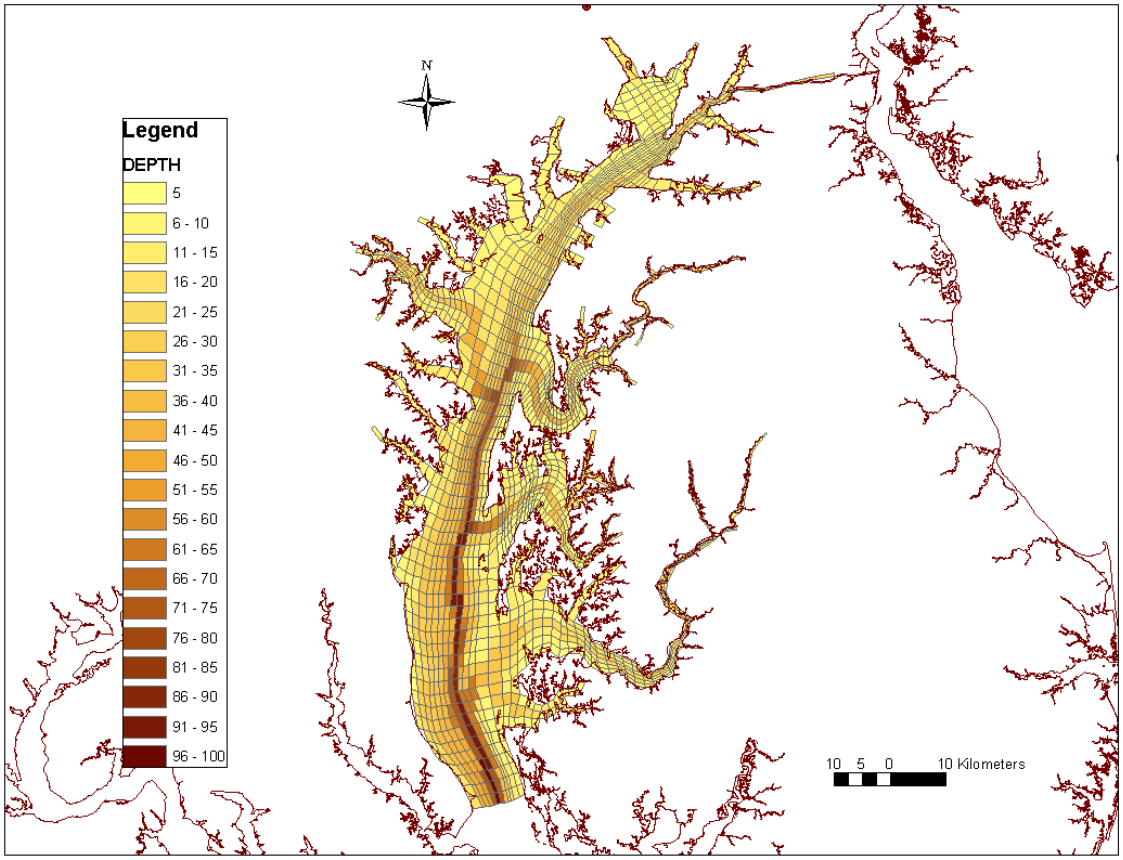

Figure 1. Surface plane of model grid.

There are 1,734 computational cells in the horizontal plane of the numerical grid with the number of maximum vertical layers of 20 (Figure 2). Of these, 427 cells are in the Chester system, including the Chester River and the Eastern Bay. Average cell length along the Chester River axis is about 1 km. Maximum number of vertical layers in the Chester estuaries is 9. Each layer is 1.52 m thick, except for the top layer, which varies with the tide and averages 2.14 m thick. The total number of computational cells is 7,917. There are 9 river inflows. Open boundary consists of 12 surface cells and total number of active cells of 107. In computation domain, there are 76 by 98 horizontal grids with 20 vertical layers.

Model Input Preparation

The geometry of the grid (file 15) and the bathymetry (file 50) were formed based on NOAA navigational chart data. Surface wind (file 14) and Surface heat flux (file 19) were taken from BWI airport meteorology data. Tide at open boundary (file 16) was from tide gage data at the Solomons Island—NOAA Gage 8577330 (Figure 3). River discharge (file 13) and temperature (file 78) were taken from USGS gages and HSPF model output. For lateral flows (file 33), both HSPF model output and point source dischargers were used. For salinity and temperature at open boundary (file 76), the data from the long-term monitoring stations CB5.1 was used. Initial salinity (file 74) and temperature (file 17) were prepared using the 1996 winter data from Chesapeake Bay Program monitoring station.

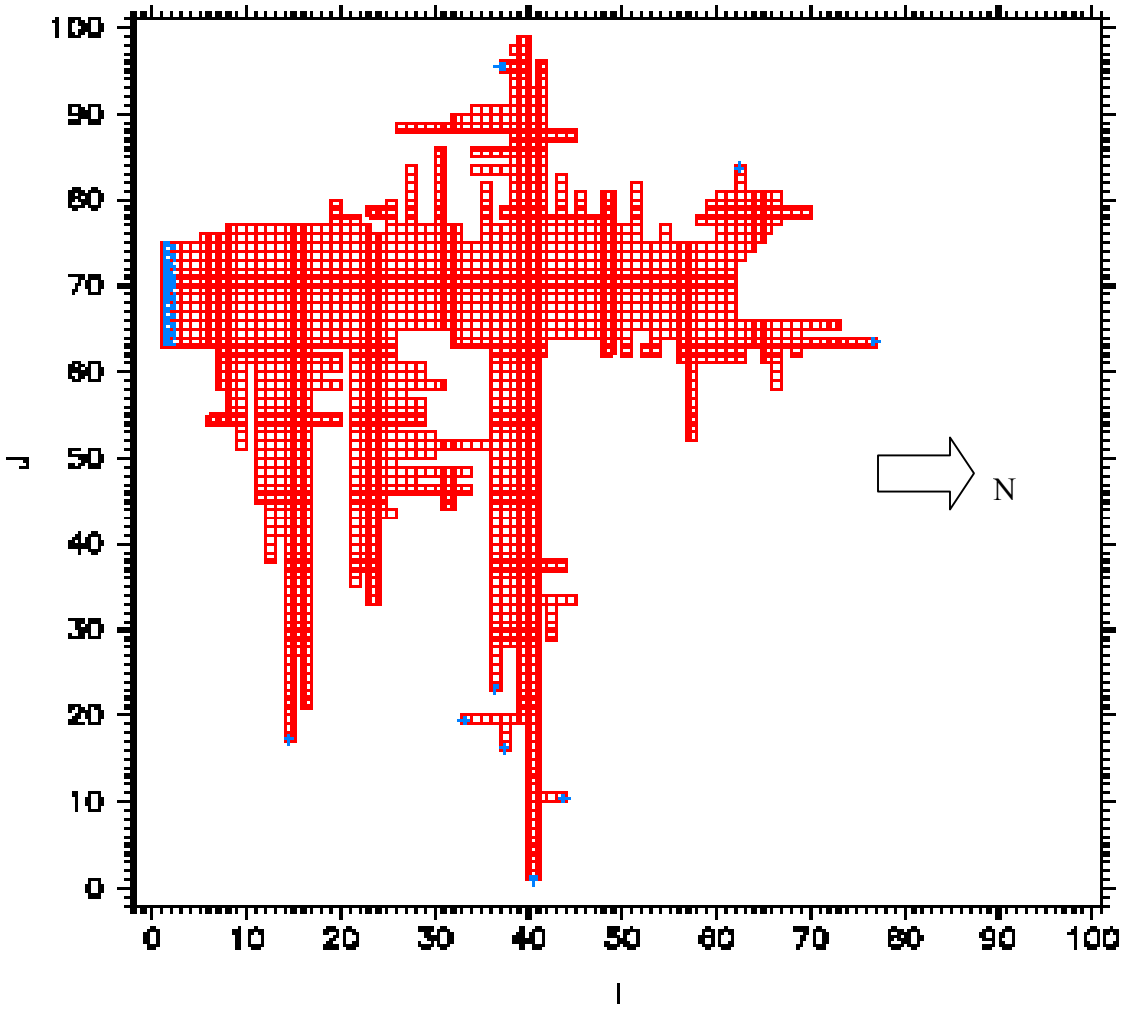

Figure 2. Surface plane of model grid in computational domain. Arrows represent freshwater inflows and circles represent open boundaries.

Model Results

Tide

Model computations were compared to observed tide at multiple stations in the upper Bay (Figure 3). One of these stations was Love Point Pier (NOAA gage 8572955), located near the mouth of the Chester River. Computed intra-tidal and inter-tidal elevations behave consistently with observation (Figure 4). Low frequency fluctuation, closely related to surface wind, captured all the meteorological events. Tidal frequency fluctuation is in good agreement in both amplitude and phase.

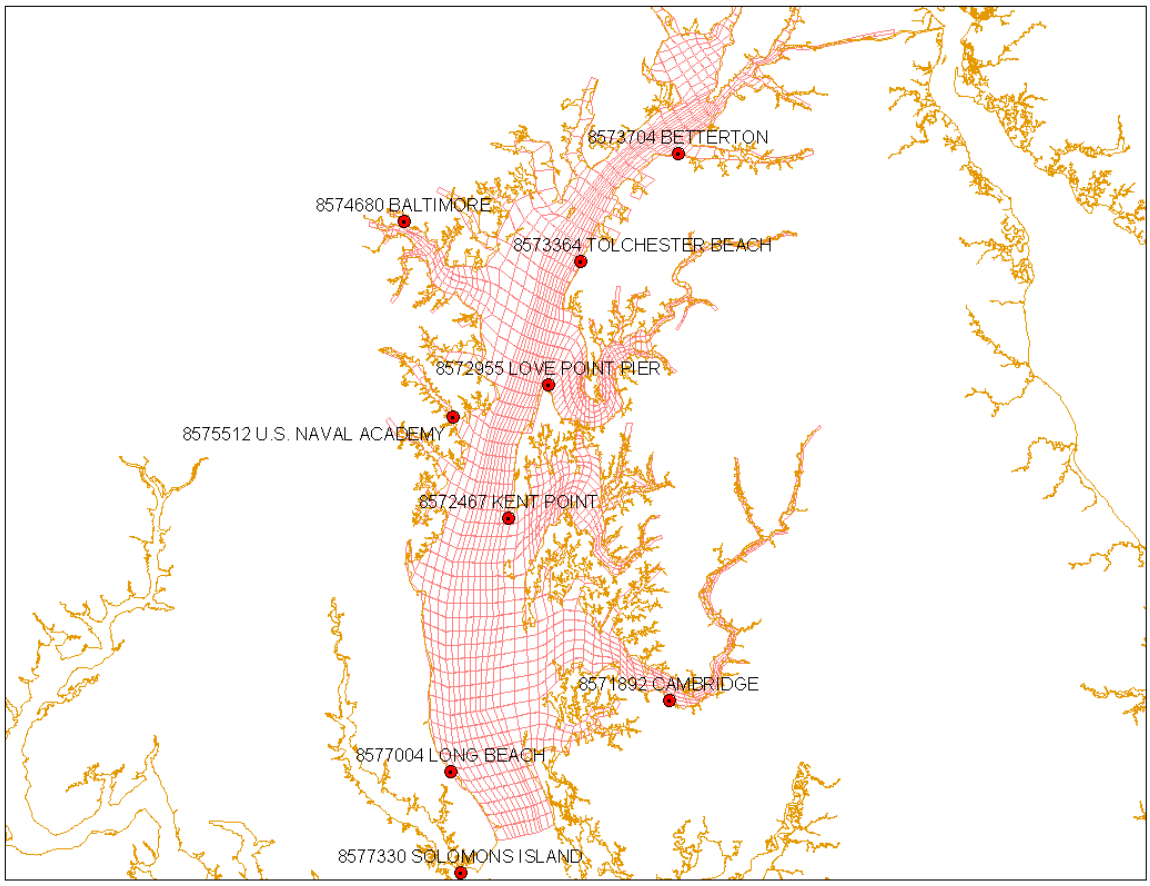

Figure 3. Tide gage locations.

Salinity

Salinity was the primary determinant of the calibration of the hydrodynamic model. This conservative substance integrates short-term and long-term effects of tides, currents, and run-off. At selected Chesapeake Bay Program long-term monitoring stations in and near the Chester system (CB3.3C, CB3.3E, CB3.3W, CB4.1C, CB4.1E, CB4.1W, EE1.1, ET4.1, ET4.2, and XGG8251), comparisons were made in a variety of

formats.

Time series (Appendix 4-A) plots of surface and bottom salinity show seasonal variations—freshening during spring and then increasing salinity until autumn. It also showed inter annual variation—wet in 1998 and dry in 1999. Also shown is more stratified water in the channel (3.3C and 4.1C) than shoals (3.3E, 3.3W, 4.1E, 4.1W). The freshwater from the Susquehanna moves south hugging western shoal, resulting fresher water in the western shoal (4.1W) than eastern shoal (4.1E). Eastern Bay (EE1.1) is closely related to the main Bay (4.1C and 4.1E). Downstream of the Chester River (ET4.2) is also influenced by the main Bay (3.3C and 3.3E) whereas the upstream (ET4.1) is controlled by the discharge from the fall line (Segment 100). The pass connecting Eastern Bay and the Chester River (XGG8251) is also well represented.

Vertical profiles (Appendix 4-B) show that the structures vary in time and space. The location of pycnocline is reasonably simulated. The mixing in upper layer is also well represented in terms of the thickness. The surface mixing is mostly controlled by the surface wind and the overall structure is dependent on turbulent mixing especially as a function of stratification. We are using an empirical approach of Bloss et al. (1988)

$$P_r = \begin{cases} P_r^{\,0} & \text{if } Ri < 0 \\ P_r^{\,0}(1+3Ri)^2 & \text{if } Ri \geq 0 \end{cases}$$

Here, Prandtl number, Pr (= ν_{ts}/ν_{tm}), relates eddy diffusivity of mass (ν_{ts}) to eddy viscosity for momentum (ν_{tm}) as a function of Richardson number, Ri (= N^2/M^2), where

$$M = \frac{\partial U}{\partial z} \quad : \text{mean velocity shear}$$

$$N^2 = \frac{\partial b}{\partial z} \quad : \text{density gradient (Bruunt - Vaisala frequency)}$$

$$b = -g\left(\frac{\rho}{\rho_0} - 1\right) \quad : \text{bouyancy}$$

In the channel of the main Bay (CB4.1C and CB3.3C), the stratification during spring and de-stratification during autumn is well simulated. In Eastern Bay entrance (EE1.1), the model is not able to simulate sudden increase of salinity near bottom in April-May (e.g., day 104 and 132). During this time period the surface mixed layer from observation is thicker than from simulation. Considering reasonable structure during the same time period in the main Bay connected to the Eastern Bay, this anomaly needs further investigation. Lower reach of the Chester River (ET4.2) shows reasonable structures.

In order to investigate the exchange between the system and the main Bay, salinity distributions along CB4.1W to EE1.1 transect was compared (Appendix 4-C).

First, it shows fresher water in the western shoal of the main Bay. It also shows that the Eastern Bay (EE1.1) is closely related to the condition in the main Bay. In general, the seasonal variation is reasonably simulated. Three-year average seasonal distributions of salinity along the channel axis of the main Bay were shown in Appendix 4-D. The seasonal cycle appears to be simulated reasonably.

Time series plots (Appendix 4-E) for the 1999 intensive survey stations by MDE show the seasonal variation is represented. The overall stratification shown by the difference between surface and bottom salinity is also reasonable. Appendix 4-F depicts the temporal variation of the longitudinal distributions along the Chester River as well as the tributaries connected to the EasternBay—Miles, Wye, and Wye East Rivers. Stratified water at the lower reach and the salt intrusion were reasonably simulated. The spatial gradient in the Chester River also appears appropriate. The discrepancy at the upstream end in Miles, Wye, and, Wye East Rivers suggests the hydrologic input from the watershed model could not be right. In summary, the hydrodynamic simulation results showed consistent temporal and spatial behavior. We are confident the hydrodynamic model provides an excellent description of transport processes within and outside the Chester River.

References

Bloss, S., R. Lehfeldt, and J. Patterson, 1988. Modeling Turbulent Transport in A Stratified Estuary. *Journal of Hydraulic Engineering,* 114, 1113-33.

Edinger, J., D. Brady, and J. Geyer. (1974). "Heat exchange and transport in the environment," Report 14, Department of Geography and Environmental Engineering, John Hopkins University, Baltimore, MD

Johnson, B.H., Kim, K.W., Heath, R.E., Hsieh, B.B., and Butler, H.L. (1991). "Development and verification of a three-dimensional numerical hydrodynamic, salinity, and temperature model of Chesapeake," Technical Report HL-91-7, US Army Engineer Waterways Experiment Station, Vicksburg, MS

Johnson, B. H., K. W. Kim, R. Heath, B. Hsieh and L. Butler. (1993). "Validation of a three-dimensional hydrodynamic model of Chesapeake Bay". *Journal of Hydraulic Engineering*, 119, 2-20.

Sheng, Y. P. (1986). "A three-dimensional mathematical model of coastal, estuarine, and lake currents using boundary-fitted grid," Report No. 585, A.R.A.P. Group of Titan Systems, Princeton, NJ.

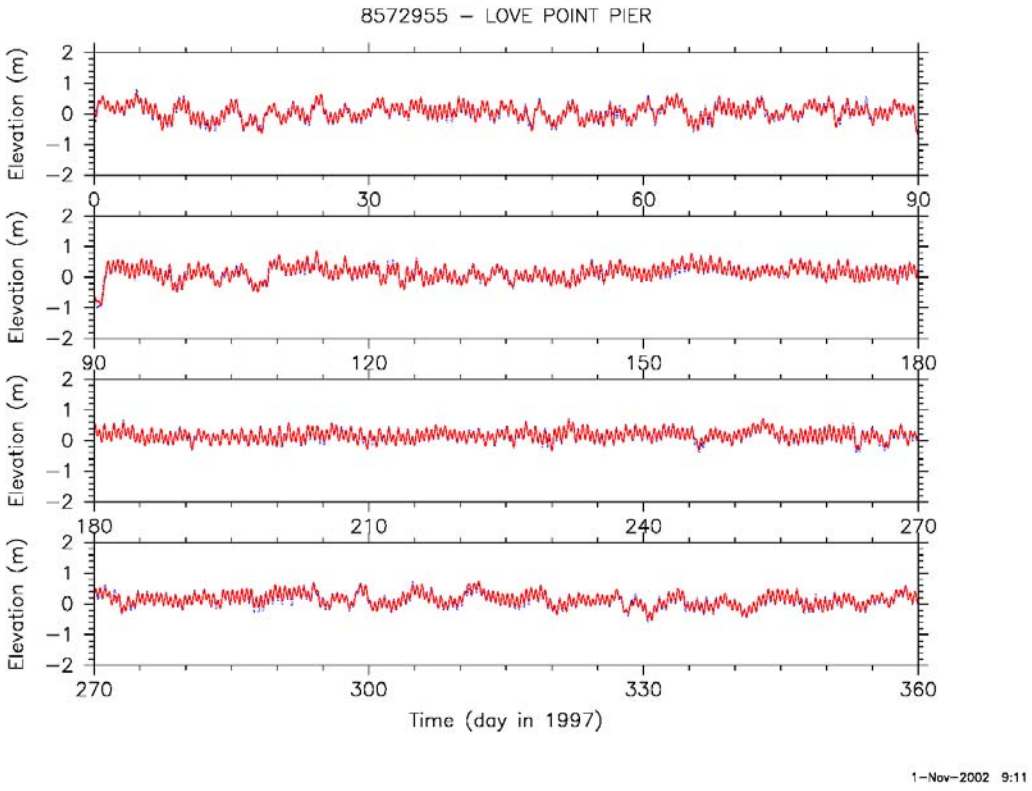

Figure 4a. Surface elevation at Love Point pier tide gage location during 1997: simulation (red) compared with tide gage observation (blue)

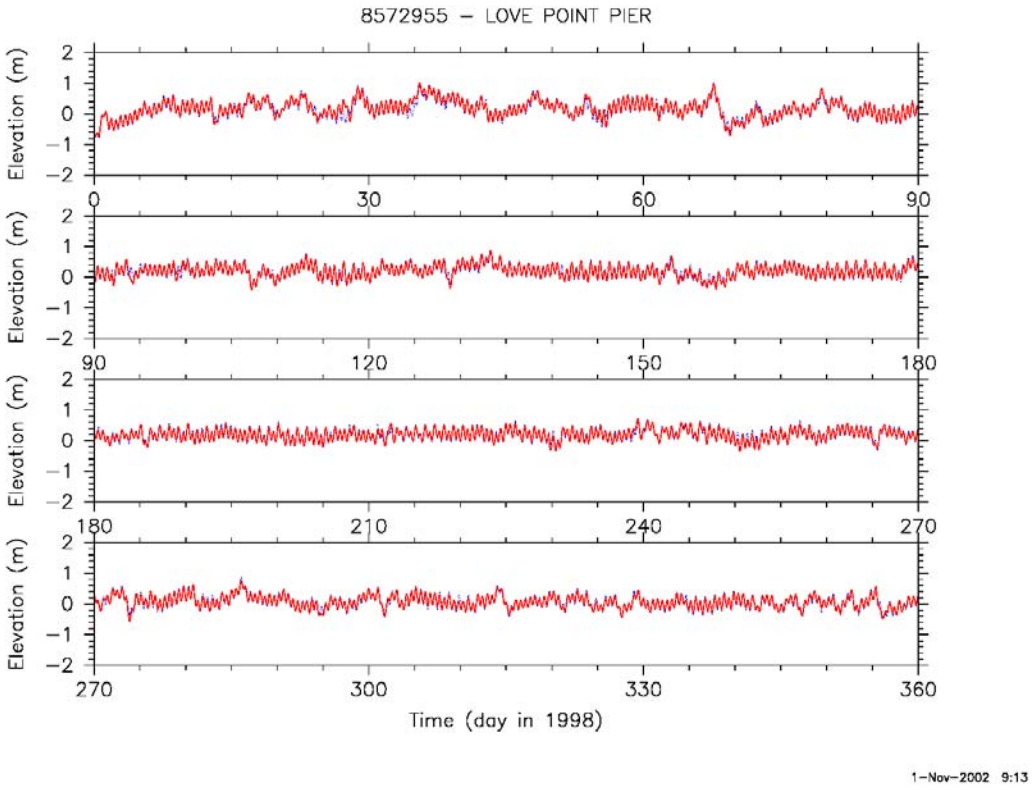

Figure 4b. Surface elevation at Love Point pier tide gage location during 1998: simulation (red) compared with tide gage observation (blue)

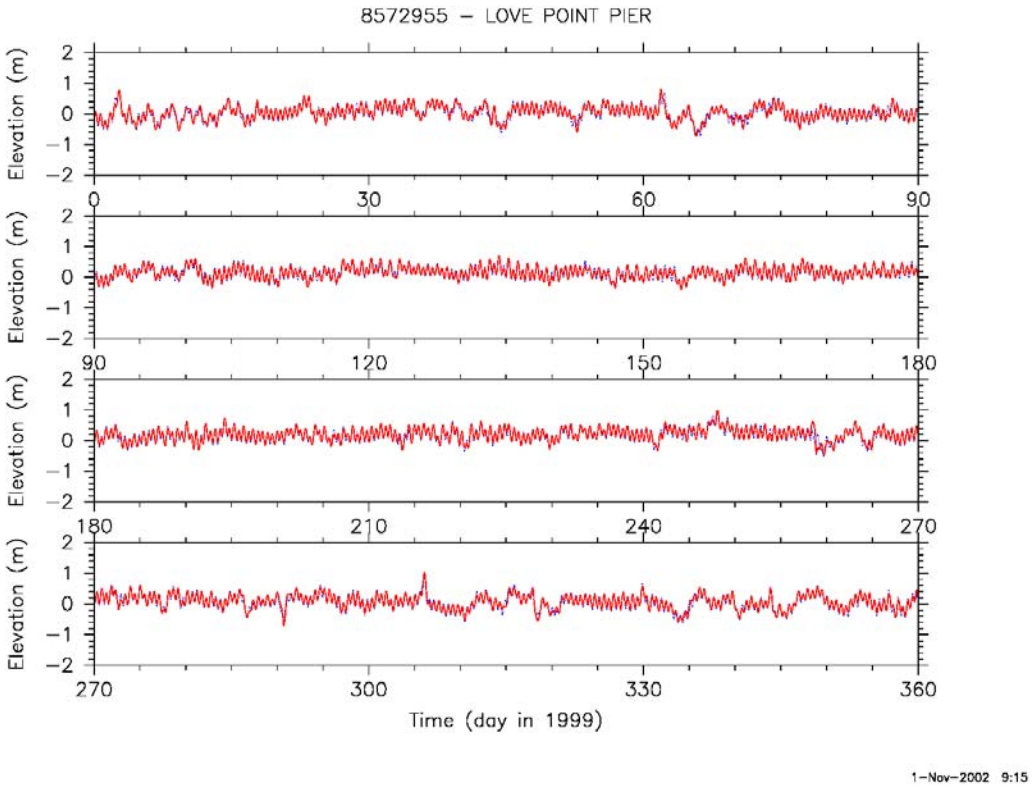

Figure 4c. Surface elevation at Love Point pier tide gage location during 1999: simulation (red) compared with tide gage observation (blue)

Appendix Figure Captions

Appendix 4-A. Time series of salinity at selected CBP long-term monitoring stations inside and adjacent the Chester system (CB3.3C, Cb3.3E, CB3.3W, CB4.1C, CB4.1E, CB4.1W, EE1.1, ET4.1, ET4.2, and XGG8251). Blue and red colors represent bottom and surface, respectively. Line denotes the CH3D simulation and cross denotes the observation.

Appendix 4-B. Vertical profiles of salinity at the same CBP stations except XGG8251 which is only one layer thick in the CH3D model. Red line and blue cross represent simulation and observation, respectively.

Appendix 4-C. Time variation of salinity exchange between the main Bay and the Eastern Bay. Along the transect from west to east, the stations are CB4.1W, CB4.1C, CB4.1E, and EE1.1. The color in circles represent observation whereas the background color represent model simulation.

Appendix 4-D. Three-year seasonal average of salinity distribution along the main Bay. Top panel represents simulation and bottom panel shows the composition of observed values.

Appendix 4-E. Time series of salinity at the MDE intensive survey stations for 1999. Red and blue lines represent simulation at surface and bottom, respectively. All the observed values at each station were shown by crosses.

Appendix 4-F. Longitudinal distribution of surface (red) and bottom (blue) salinity during each intensive survey period in the Chester system. Four major river axes were shown: Chester River, Miles River, Wye River, and Wye East River. Dotted lines represent maximum and minimum values during the period.

5 Water Quality Model Formulation

Introduction

CE-QUAL-ICM was designed to be a flexible, widely-applicable eutrophication model. Initial application was to Chesapeake Bay (Cerco and Cole 1994). Subsequent additional applications included the Delaware Inland Bays (Cerco et al. 1994), Newark Bay (Cerco and Bunch 1997), and the San Juan Estuary (Bunch et al. 2000). Each model application employed a different combination of model features and required addition of system-specific capabilities. This chapter describes general features and site-specific developments of the model as presently applied to the water column of Chesapeake Bay.

Conservation of Mass Equation

The foundation of CE-QUAL-ICM is the solution to the three-dimensional mass-conservation equation for a control volume. Control volumes correspond to cells on the model grid. CE-QUAL-ICM solves, for each volume and for each state variable, the equation:

$$\frac{\delta V_j \bullet C_j}{\delta t} = \sum_{k=1}^{n} Q_k \bullet C_k + \sum_{k=1}^{n} A_k \bullet D_k \bullet \frac{\delta C}{\delta x_k} + \Sigma S_j \qquad (1)$$

in which:

V_j = volume of j^{th} control volume (m^3)
C_j = concentration in j^{th} control volume (g m^{-3})
t, x = temporal and spatial coordinates
n = number of flow faces attached to j^{th} control volume
Q_k = volumetric flow across flow face k of j^{th} control volume (m^3 s^{-1})
C_k = concentration in flow across face k (g m^{-3})
A_k = area of flow face k (m^2)
D_k = diffusion coefficient at flow face k (m^2 s^{-1})
S_j = external loads and kinetic sources and sinks in j^{th} control volume (g s^{-1})

Solution of Equation 1 on a digital computer requires discretization of

the continuous derivatives and specification of parameter values. The equation is solved using the QUICKEST algorithm (Leonard 1979) in the horizontal plane and a Crank-Nicolson scheme in the vertical direction. Discrete time steps, determined by computational stability requirements, are ≈15 minutes.

State Variables

At present, the CE-QUAL-ICM model incorporates 24 state variables in the water column including physical variables, multiple algal groups, two zooplankton groups, and multiple forms of carbon, nitrogen, phosphorus and silica (Table 1).

Algae

Algae are grouped into three model classes. In the complete Chesapeake Bay model, these are cyanobacteria, spring diatoms, and greens. The grouping is based upon the distinctive characteristics of each class and upon the significant role the characteristics play in the ecosystem. The cyanobacteria distinguished in the complete model are the bloom-forming species found in the tidal, freshwater Potomac River. For the Chester application, we substituted a distinct freshwater Chester algal group for the Potomac cyanobacteria. Based on dissolved silica observations, the freshwater Chester algae appear to be diatoms. Flexibility built into the model allows this substitution with no difficulty. Spring diatoms are large phytoplankton that produce an annual bloom in the saline portions of the bay and tributaries. Settling of spring diatom blooms to the sediments may be a significant source of carbon for sediment oxygen demand. Diatoms are distinguished by their requirement of silica as a nutrient to form cell walls. Algae that do not fall into the preceding two groups are lumped into the heading of green algae. The green algae represent the mixture that characterizes saline waters during summer and autumn and fresh waters in the remaining tributaries year round. Non-bloom forming diatoms comprise a portion of this mixture.

Zooplankton

Two zooplankton groups are considered: microzooplankton and mesozooplankton. The microzooplankton can be important predators on phytoplankton and they are one of the prey groups for mesozooplankton. Mesozooplankton consume phytoplankton and detritus as well as microzooplankton. The mesozooplankton are an important prey resource for carnivorous finfish such as Bay Anchovy. Zooplankton were included in the model as a first step towards computing the effect of eutrophication management on top-level predators.

Organic Carbon

Three organic carbon state variables are considered: dissolved, labile particulate, and refractory particulate. Labile and refractory distinctions are based upon the time scale of decomposition. Labile organic carbon decomposes on a time scale of days to weeks while refractory organic carbon requires more time. Labile organic carbon decomposes rapidly in the water column or the sediments. Refractory organic carbon decomposes slowly, primarily in the sediments, and may contribute to sediment oxygen demand years after deposition.

Nitrogen

Nitrogen is first divided into available and unavailable fractions. Available refers to employment in algal nutrition. Two available forms are considered: reduced and oxidized nitrogen. Reduced nitrogen includes ammonium and urea. Nitrate and nitrite comprise the oxidized nitrogen pool. Both reduced and oxidized nitrogen are utilized to fulfill algal nutrient requirements. The primary reason for distinguishing the two is that ammonium is oxidized by nitrifying bacteria into nitrite and, subsequently, nitrate. This oxidation can be a significant sink of oxygen in the water column and sediments.

Unavailable nitrogen state variables are dissolved organic nitrogen, labile particulate organic nitrogen, and refractory particulate organic nitrogen. The dissolved organic nitrogen state variable excludes urea which is directly available as an algal nutrient.

Phosphorus

As with nitrogen, phosphorus is first divided into available and unavailable fractions. Only a single available form, dissolved phosphate, is considered. The model framework allows for exchange of phosphate between dissolved and particulate (sorbed to solids) forms but this option is not implemented in the present application. Three forms of unavailable phosphorus are considered: dissolved organic phosphorus, labile particulate organic phosphorus, and refractory particulate organic phosphorus.

Silica

Silica is divided into two state variables: dissolved silica and particulate biogenic silica. Dissolved silica is available to diatoms while particulate biogenic silica cannot be utilized. In the model, particulate biogenic silica is produced through diatom mortality. Particulate biogenic silica undergoes dissolution to available silica or else settles to the bottom sediments.

Chemical Oxygen Demand

Chemical oxygen demand is the concentration of reduced substances that are oxidized by abiotic processes. The primary component of chemical oxygen demand is sulfide released from sediments. Oxidation of sulfide to sulfate may remove substantial quantities of dissolved oxygen from the water column.

Dissolved Oxygen

Dissolved oxygen is required for the existence of higher life forms. Oxygen availability determines the distribution of organisms and the flows of energy and nutrients in an ecosystem. Dissolved oxygen is a central component of the water-quality model.

Salinity

Salinity is a conservative tracer that provides verification of the transport component of the model and facilitates examination of conservation of mass. Salinity also influences the dissolved oxygen saturation concentration and may be used in the determination of kinetics constants that differ in saline and fresh water.

Temperature

Temperature is a primary determinant of the rate of biochemical reactions. Reaction rates increase as a function of temperature although extreme temperatures may result in the mortality of organisms and a decrease in kinetics rates.

Fixed Solids

Fixed solids are the mineral fraction of total suspended solids. Solids are considered primarily for their role in light attenuation.

The remainder of this chapter is devoted to detailing the kinetics sources and sinks and to reporting parameter values. For notational simplicity, the transport terms are dropped in the reporting of kinetics formulations.

Algae

Equations governing the three algal groups are largely the same. Differences among groups are expressed through the magnitudes of parameters in the equations. Generic equations are presented below except when group-specific relationships are required.

Algal sources and sinks in the conservation equation include production, metabolism, predation, and settling. These are expressed:

$$\frac{\delta}{\delta t} B = \left(G - BM - Wa \bullet \frac{\delta}{\delta z} \right) B - PR \quad (2)$$

in which:

B = algal biomass, expressed as carbon (g C m^{-3})
G = growth (d^{-1})
BM = basal metabolism (d^{-1})
Wa = algal settling velocity (m d^{-1})
PR = predation (g C m^{-3} d^{-1})
z = vertical coordinate

Production

Production by phytoplankton is determined by the intensity of light, by the availability of nutrients, and by the ambient temperature.

Light

The influence of light on phytoplankton production is represented by a chlorophyll-specific production equation (Jassby and Platt 1976):

$$P^B = P^B m \frac{I}{\sqrt{I^2 + Ik^2}} \quad (3)$$

in which:

P^B = photosynthetic rate (g C g^{-1} Chl d^{-1})
$P^B m$ = maximum photosynthetic rate (g C g^{-1} Chl d^{-1})
I = irradiance (E m^{-2} d^{-1})

Parameter Ik is defined as the irradiance at which the initial slope of the production vs. irradiance relationship (Figure 1) intersects the value of $P^B m$

$$Ik = \frac{P^B m}{\alpha} \quad (4)$$

in which:

α = initial slope of production vs. irradiance relationship (g C g^{-1} Chl (E m^{-2})$^{-1}$)

Chlorophyll-specific production rate is readily converted to carbon specific growth rate, for use in Equation 2, through division by the carbon-to-chlorophyll ratio:

$$G = \frac{P^B}{CChl} \quad (5)$$

in which:

CChl = carbon-to-chlorophyll ratio (g C g^{-1} chlorophyll a)

Specification of the carbon-to-chlorophyll ratio is based on observations collected as part of the phytoplankton monitoring program.

Nutrients

Carbon, nitrogen, and phosphorus are the primary nutrients required for algal growth. Diatoms require silica, as well. Inorganic carbon is usually available in excess and is not considered in the model. The effects of the remaining nutrients on growth are described by the formulation commonly referred to as "Monod kinetics" (Figure 2; Monod 1949):

$$f(N) = \frac{D}{KHd + D} \quad (6)$$

in which:

f(N) = nutrient limitation on algal production ($0 \leq f(N) \leq 1$)
D = concentration of dissolved nutrient (g m^{-3})
KHd = half-saturation constant for nutrient uptake (g m^{-3})

Temperature

Algal production increases as a function of temperature until an optimum temperature or temperature range is reached. Above the optimum, production declines until a temperature lethal to the organisms is attained. Numerous functional representations of temperature effects are available. Inspection of growth versus temperature data indicates a function similar to a Gaussian probability curve (Figure 3) provides a good fit to observations:

$$f(T) = e^{-KTg1 \bullet (T - Topt)^2} \; when \; T \leq Topt$$

$$= e^{-KTg2 \bullet (Topt - T)^2} \; when \; T > Topt \quad (7)$$

in which:

T = temperature (^oC)
Topt = optimal temperature for algal growth (^oC)
KTg1 = effect of temperature below Topt on growth ($^oC^{-2}$)
KTg2 = effect of temperature above Topt on growth ($^oC^{-2}$)

Constructing the Photosynthesis vs. Irradiance Curve

A production versus irradiance relationship is constructed for each model cell at each time step. First, the maximum photosynthetic rate under ambient temperature and nutrient concentrations is determined:

$$P^B m(N,T) = P^B m \bullet f(T) \bullet \frac{D}{KHd + D} \tag{8}$$

in which:

$P^B m(N,T)$ = maximum photosynthetic rate under ambient temperature and nutrient concentrations (g C g^{-1} Chl d^{-1})

The single most limiting nutrient is employed in determining the nutrient limitation.

Next, parameter Ik is derived from Equation 4. Finally, the production vs. irradiance relationship is constructed using $P^B m(N,T)$ and Ik. The resulting production versus irradiance curve exhibits three regions (Figure 4). For I >> Ik, the value of the term $I / (I^2 + Ik^2)^{½}$ approaches unity and temperature and nutrients are the primary factors that influence production. For I << Ik, production is determined solely by α and irradiance I. In the region where the initial slope of the production versus irradiance curve intercepts the line indicating production at optimal illumination, I ≈ Ik, production is determined by the combined effects of temperature, nutrients, and light.

Irradiance

Irradiance at the water surface is evaluated at each model time step. Instantaneous irradiance is computed by fitting a sin function to daily total irradiance:

$$Io = \frac{\Pi}{2 \bullet FD} \bullet IT \bullet \sin\left(\frac{\Pi \bullet DSSR}{FD}\right) \tag{9}$$

in which:

Io = irradiance at water surface (E m^{-2} d^{-1})
IT = daily total irradiance (E m^{-2})
FD = fractional daylength ($0 \leq FD \leq 1$)
DSSR = time since sunrise (d)

Io is evaluated only during the interval:

$$\frac{1 - FD}{2} \le DSM \le \frac{1 + FD}{2} \quad (10)$$

in which:

DSM = time since midnight (d)

Outside the specified interval, Io is set to zero.

Irradiance declines exponentially with depth below the surface. The diffuse attenuation coefficient, Kd, is computed as a function of color and concentrations of organic and mineral solids.

Respiration

Two forms of respiration are considered in the model: photo-respiration and basal metabolism. Photo-respiration represents the energy expended by carbon fixation and is a fixed fraction of production. In the event of no production (e.g. at night), photo-respiration is zero. Basal metabolism is a continuous energy expenditure to maintain basic life processes. In the model, metabolism is considered to be an exponentially increasing function of temperature (Figure 5). Total respiration is represented:

$$R = Presp \bullet G + BM \bullet e^{KTb \bullet (T - Tr)} \quad (11)$$

in which:

Presp = photo-respiration ($0 \le Presp \le 1$)
BM = metabolic rate at reference temperature Tr (d^{-1})
KTb = effect of temperature on metabolism ($^oC^{-1}$)
Tr = reference temperature for metabolism (^oC)

Predation

The predation term includes the activity of zooplankton, filter-feeding benthos, and other pelagic filter feeders including planktivorous fish. Formulation and results of the zooplankton computation appear in Cerco and Noel, 2003). Details of the benthos computations may be found in HydroQual (2000) and at http://www.chesapeakebay.net/model.htm. Predation by other planktivores is modeled by assuming predators clear a specific volume of water per unit biomass:

$$PR = F \bullet B \bullet M \quad (12)$$

F = filtration rate ($m^3\ g^{-1}$ predator C d^{-1})
M = planktivore biomass (g C m^{-3})

Detailed specification of the spatial and temporal distribution of the predator population is impossible. One approach is to assume predator biomass is proportional to algal biomass, $M = \gamma B$, in which case Equation 12 can be rewritten:

$$PR = \gamma \bullet F \bullet B^2 \quad (13)$$

Since neither γ nor F are known precisely, the logical approach is to combine their product into a single unknown determined during the model calibration procedure. Effect of temperature on predation is represented with the same formulation as the effect of temperature on respiration. The final representation of predation, including zooplankton, is:

$$PR = \frac{B}{KHsz + B} \bullet RMsz \bullet SZ + \frac{B}{KHlz + B} \bullet RMlz \bullet LZ + Phtl \bullet B^2 \quad (14)$$

RMsz = microzooplankton maximum ration (g algal C g^{-1} zoo C d^{-1})
SZ = microzooplankton biomass (g C m^{-3})
KHsz = half saturation concentration for carbon uptake by microzooplankton (g C m^{-3})
RMlz = mesozooplankton maximum ration (g algal C g^{-1} zoo C d^{-1})
LZ = mesozooplankton biomass (g C m^{-3})
KHlz = half saturation concentration for carbon uptake by mesozooplankton (g C m^{-3})
Phtl = rate of predation by other planktivores (m^3 g^{-1} C d^{-1})

Predation by filter-feeding benthos is represented as a loss term only in model cells that intersect the bottom.

Accounting for Algal Phosphorus

The amount of phosphorus incorporated in algal biomass is quantified through a stoichiometric ratio. Thus, total phosphorus in the model is expressed:

$$TotP = PO_4 + Apc - B + DOP + LPOP + RPOP \quad (15)$$

TotP = total phosphorus (g P m^{-3})
PO_4 = dissolved phosphate (g P m^{-3})
Apc = algal phosphorus-to-carbon ratio (g P g^{-1} C)
DOP = dissolved organic phosphorus (g P m^{-3})
LPP = labile particulate organic phosphorus (g P m^{-3})
RPP = refractory particulate organic phosphorus (g P m^{-3})

Algae take up dissolved phosphate during production and release dissolved phosphate and organic phosphorus through respiration. The fate of phosphorus released by respiration is determined by empirical distribution coefficients. The fate of algal phosphorus recycled by predation is determined by

a second set of distribution parameters.

Accounting for Algal Nitrogen

Model nitrogen state variables include ammonium+urea, nitrate+nitrite, dissolved organic nitrogen, labile particulate organic nitrogen, and refractory particulate organic nitrogen. The amount of nitrogen incorporated in algal biomass is quantified through a stoichiometric ratio. Thus, total nitrogen in the model is expressed:

$$TotN = NH_4\text{-}Urea + NO_{23} + Anc\_B + DON + LPON + RPON \qquad (16)$$

TotN = total nitrogen (g N m^{-3})
NH_4-Urea = ammonium+urea (g N m^{-3})
NO_{23} = nitrate+nitrite (g N m^{-3})
Anc = algal nitrogen-to-carbon ratio (g N g^{-1} C)
DON = dissolved organic nitrogen (g N m^{-3})
LPON = labile particulate organic nitrogen (g N m^{-3})
RPON = refractory particulate organic nitrogen (g N m^{-3})

As with phosphorus, the fate of algal nitrogen released by metabolism and predation is represented by distribution coefficients.

Algal Nitrogen Preference

Algae take up ammonium+urea and nitrate+nitrite during production and release ammonium+urea and organic nitrogen through respiration. Nitrate+nitrite is internally reduced to ammonium before synthesis into biomass occurs (Parsons et al. 1984). Trace concentrations of ammonium+urea inhibit nitrate reduction so that, in the presence of multiple nitrogenous nutrients, ammonium+urea is utilized first. The "preference" of algae for ammonium+urea is expressed by an empirical function (Thomann and Fitzpatrick 1982):

$$PN = NH_4\text{-}Urea \bullet \frac{NO_{23}}{(KHn + NH_4\text{-}Urea) \bullet (KHn + NO_{23})} + NH_4\text{-}Urea \bullet \frac{KHn}{(NH_4\text{-}Urea + NO_{23}) \bullet (KHn + NO_{23})} \qquad (17)$$

in which

PN = algal preference for ammonium uptake ($0 \leq Pn \leq 1$)
KHn = half saturation concentration for algal nitrogen uptake (g N m^{-3})

The function has two limiting values (Figure 6). When nitrate+nitrite is absent, the preference for ammonium+urea is unity. When ammonium+urea is absent, the preference is zero. In the presence of ammonium+urea and nitrate+nitrite, the preference depends on the abundance of both forms relative to

the half-saturation constant for nitrogen uptake. When both ammonium+urea and nitrate+nitrite are abundant, the preference for ammonium+urea approaches unity. When ammonium+urea is scarce but nitrate+nitrite is abundant, the preference decreases in magnitude and a significant fraction of algal nitrogen requirement comes from nitrate+nitrite.

Effect of Algae on Dissolved Oxygen

Algae produce oxygen during photosynthesis and consume oxygen through respiration. The quantity produced depends on the form of nitrogen utilized for growth. More oxygen is produced, per unit of carbon fixed, when nitrate is the algal nitrogen source than when ammonium is the source. Equations describing algal uptake of carbon and nitrogen and production of dissolved oxygen (Morel 1983) are:

$$106\,CO_2 + 16\,NH_4^+ + H_2PO_4^- + 106\,H_2O \rightarrow \text{protoplasm} + 106\,O_2 + 15\,H^+ \quad (18)$$

$$106\,CO_2 + 16\,NO_3^- + H_2PO_4^- + 122\,H_2O + 17\,H^+ \rightarrow \text{protoplasm} + 138\,O_2 \quad (19)$$

When ammonium is the nitrogen source, one mole oxygen is produced per mole carbon dioxide fixed. When nitrate is the nitrogen source, 1.3 moles oxygen are produced per mole carbon dioxide fixed.

The equation that describes the effect of algae on dissolved oxygen in the model is:

$$\frac{\delta}{\delta t} DO = \left[(1.3 - 0.3 \bullet PN) \bullet P - (1 - FCD) \bullet BM\right] \bullet AOCR \bullet B \quad (20)$$

in which:

FCD = fraction of algal metabolism recycled as dissolved organic carbon ($0 \leq FCD \leq 1$)
AOCR = dissolved oxygen-to-carbon ratio in respiration (2.67 g O_2 g^{-1} C)

The magnitude of AOCR is derived from a simple representation of the respiration process:

$$CH_2O + O_2 = CO_2 + H_2O \quad (21)$$

The quantity (1.3 - 0.3 × PN) is the photosynthesis ratio and expresses the molar quantity of oxygen produced per mole carbon fixed. The photosynthesis ratio approaches unity as the algal preference for ammonium

approaches unity.

Accounting for Algal Silica

The amount of silica incorporated in algal biomass is quantified through a stoichiometric ratio. Thus, total silica in the model is expressed:

$$\text{TotSi} = \text{Dsil} + \text{Asc\_B} + \text{PBS} \tag{22}$$

TotSi = total silica (g Si m^{-3})
Dsil = dissolved silica (g Si m^{-3})
Asc = algal silica-to-carbon ratio (g Si g^{-1} C)
PBS = particulate biogenic silica (g Si m^{-3})

As with the other nutrients, the fate of algal silica released by metabolism and predation is represented by distribution coefficients.

Salinity Toxicity

The Group 1 algae represented in the model are freshwater organisms that cease production when salinity exceeds 1 to 2 ppt (Sellner et al. 1988). The effect of salinity on Group 1 algae was represented by a mortality term in the form of a rectangular hyperbola:

$$STOX1 = STF1 \bullet \frac{S}{KHst1 + S} \tag{23}$$

in which

STOX1 = mortality induced by salinity on Group 1 algae (d^{-1})
STF1 = maximum salinity mortality on Group 1 algae (d^{-1})
S = salinity (ppt)
KHst1 = salinity at which mortality is half maximum value (ppt)

The spring diatom bloom is limited to saline water. The limiting mechanism is not defined but appears to be related to salinity. The upstream limit of the spring bloom was defined in the model by introducing a mortality term at low salinity:

$$STOX2 = STF2 \bullet KHst\frac{2}{KHst2 + S} \tag{24}$$

in which

STOX2 = mortality induced by freshwater on spring diatoms (d^{-1})
STF2 = maximum freshwater mortality on spring diatoms (d^{-1})

S = salinity (ppt)
KHst2 = salinity at which mortality is half maximum value (ppt)

The salinity-related mortality (Figure 7) is added to the basal metabolism.

Organic Carbon

Organic carbon undergoes innumerable transformations in the water column. The model carbon cycle (Figure 8) consists of the following elements:

Phytoplankton production and excretion
Zooplankton production and excretion
Predation on phytoplankton
Dissolution of particulate carbon
Heterotrophic respiration
Denitrification
Settling

Algal production is the primary carbon source although carbon also enters the system through external loading. Predation on algae by zooplankton and other organisms releases particulate and dissolved organic carbon to the water column. A fraction of the particulate organic carbon undergoes first-order dissolution to dissolved organic carbon. Dissolved organic carbon produced by excretion, by predation, and by dissolution is respired at a first-order rate to inorganic carbon. Particulate organic carbon which does not undergo dissolution settles to the bottom sediments.

Zooplankton kinetics are detailed in Cerco and Noel (2003). Kinetics of the organic carbon state variables are described below.

Dissolution and Respiration

Organic carbon dissolution and respiration are represented as first-order processes in which the reaction rate is proportional to concentration of the reactant. An exponential function (Figure 5) relates dissolution and respiration to temperature.

In the model, a Monod-like function diminishes respiration as dissolved oxygen approaches zero. As oxygen is depleted from natural systems, oxidation of organic matter is effected by the reduction of alternate oxidants. The sequence in which alternate oxidants are employed is determined by the thermodynamics of oxidation-reduction reactions. The first substance reduced in the absence of oxygen is nitrate. A representation of the denitrification reaction can be obtained by balancing standard half-cell redox reactions (Stumm and Morgan 1981):

$$4\,NO_3^- + 4\,H^+ + 5\,CH_2O \rightarrow 2\,N_2 + 7\,H_2O + 5\,CO_2 \qquad (25)$$

Equation 25 describes the stoichiometry of the denitrification reaction. The kinetics of the reaction, represented in the model, are first-order. The dissolved organic carbon respiration rate, Kdoc, is modified so that significant decay via denitrification occurs only when nitrate is freely available and dissolved oxygen is depleted (Figure 9). A parameter is included so that the anoxic respiration rate is slower than oxic respiration:

$$Denit = \frac{KHodoc}{KHodoc + DO} \bullet \frac{NO_3}{KHndn + NO_3} \bullet AANOX \bullet Kdoc \qquad (26)$$

in which:

Denit = denitrification rate of dissolved organic carbon (d^{-1})
Kdoc = first-order dissolved organic carbon respiration rate (d^{-1})
AANOX = ratio of denitrification to oxic carbon respiration rate
($0 \leq AANOX \leq 1$)
KHodoc = half-saturation concentration of dissolved oxygen required for oxic respiration ($g\ O_2\ m^{-3}$)
KHndn = half-saturation concentration of nitrate required for denitrification ($g\ N\ m^{-3}$)

Dissolved Organic Carbon

The complete representation of dissolved organic carbon sources and sinks in the model ecosystem is:

$$\frac{\delta}{\delta t} DOC = FCD \bullet R \bullet B + FCDP \bullet PR + Klpoc \bullet LPOC + Krpoc \bullet RPOC - \frac{DO}{KHodoc + DO} \bullet Kdoc \bullet DOC - DENIT \bullet DOC \qquad (27)$$

in which:

DOC = dissolved organic carbon ($g\ m^{-3}$)
LPOC = labile particulate organic carbon ($g\ m^{-3}$)
RPOC = refractory particulate organic carbon ($g\ m^{-3}$)
FCD = fraction of algal respiration released as DOC ($0 < FCD < 1$)
FCDP = fraction of predation on algae released as DOC ($0 < FCDP < 1$)
Klpoc = dissolution rate of LPOC (d^{-1})
Krpoc = dissolution rate of RPOC (d^{-1})
Kdoc = respiration rate of DOC (d^{-1})

Labile Particulate Organic Carbon

The complete representation of labile particulate organic carbon sources and sinks in the model ecosystem is:

$$\frac{\delta}{\delta t} LPOC = FCL \bullet R \bullet B + FCLP \bullet PR - Klpoc \bullet LPOC - Wl \bullet \frac{\delta}{\delta z} LPOC \quad (28)$$

in which:

FCL = fraction of algal respiration released as LPOC (0 < FCL < 1)
FCLP = fraction of predation on algae released as LPOC (0 < FCLP < 1)
Wl = settling velocity of labile particles (m d^{-1})

Refractory Particulate Organic Carbon

The complete representation of refractory particulate organic carbon sources and sinks in the model ecosystem is:

$$\frac{\delta}{\delta t} RPOC = FCR \bullet R \bullet B + FCRP \bullet PR - Krpoc \bullet RPOC - Wr \bullet \frac{\delta}{\delta z} RPOC \quad (29)$$

in which:

FCR = fraction of algal respiration released as RPOC (0 < FCR < 1)
FCRP = fraction of predation on algae released as RPOC (0 < FCRP < 1)
Wr = settling velocity of refractory particles (m d^{-1})

Phosphorus

The model phosphorus cycle (Figure 10) includes the following processes:

Algal uptake and excretion
Zooplankton excretion
Predation
Hydrolysis of particulate organic phosphorus
Mineralization of dissolved organic phosphorus
Settling and resuspension

External loads provide the ultimate source of phosphorus to the system. Dissolved phosphate is incorporated by algae during growth and released as phosphate and organic phosphorus through respiration and predation. Dissolved organic phosphorus is mineralized to phosphate. A portion of the particulate organic phosphorus hydrolyzes to dissolved organic phosphorus. The balance settles to the sediments. Within the sediments, particulate phosphorus is mineralized and recycled to the water column as dissolved phosphate.

Hydrolysis and Mineralization

Within the model, hydrolysis is defined as the process by which particulate organic substances are converted to dissolved organic form. Mineralization is defined as the process by which dissolved organic substances are converted to dissolved inorganic form. Conversion of particulate organic phosphorus to phosphate proceeds through the sequence of hydrolysis and mineralization. Direct mineralization of particulate organic phosphorus does not occur.

Mineralization of organic phosphorus is mediated by the release of nucleotidase and phosphatase enzymes by bacteria (Ammerman and Azam 1985; Chrost and Overbeck 1987) and algae (Matavulj and Flint 1987; Chrost and Overbeck 1987; Boni et al. 1989). Since the algae themselves release the enzyme and since bacterial abundance is related to algal biomass, the rate of organic phosphorus mineralization is related, in the model, to algal biomass. A most remarkable property of the enzyme process is that alkaline phosphatase activity is inversely proportional to ambient phosphate concentration (Chrost and Overbeck 1987; Boni et al. 1989). Put in different terms, when phosphate is scarce, algae stimulate production of an enzyme that mineralizes organic phosphorus to phosphate. This phenomenon is simulated by relating mineralization to the algal phosphorus nutrient limitation. Mineralization is highest when algae are strongly phosphorus limited and is least when no limitation occurs.

The expression for mineralization rate is:

$$Kdop = Kdp + \frac{KHp}{KHp + PO_4} \bullet Kdpalg \bullet B \qquad (30)$$

in which:

Kdop = mineralization rate of dissolved organic phosphorus (d^{-1})
Kdp = minimum mineralization rate (d^{-1})
KHp = half-saturation concentration for algal phosphorus uptake (g P m^{-3})
PO_4 = dissolved phosphate (g P m^{-3})
Kdpalg = constant that relates mineralization to algal biomass (m^3 g^{-1} C d^{-1})

Potential effects of algal biomass and nutrient limitation on the mineralization rate are shown in Figure 11. When nutrient concentration greatly exceeds the half-saturation concentration for algal uptake, the rate roughly equals the minimum. Algal biomass has little influence. As nutrient becomes scarce relative to the half-saturation concentration, the rate increases. The magnitude of the increase depends on algal biomass. Factor of two to three increases are feasible.

Exponential functions (Figure 4) relate mineralization and hydrolysis rates to temperature.

Precipitation and Bacterial Uptake

Functions to represent precipitation and uptake by sulfide-oxidizing bacteria were added during the model calibration procedure. These functions are described in Cerco and Noel (2003).

Dissolved Phosphate

The mass-balance equation for dissolved phosphate is:

$$\frac{\delta}{\delta t} PO_4 = Kdop \bullet DOP - APC \bullet G \bullet B + APC \bullet \left[FPI \bullet BM \bullet B + FPIP \bullet PR \right] \tag{31}$$

in which:

FPI = fraction of algal metabolism released as dissolved phosphate ($0 \leq FPI \leq 1$)
FPIP = fraction of predation released as dissolved phosphate ($0 \leq FPIP \leq 1$)

Dissolved Organic Phosphorus

The mass balance equation for dissolved organic phosphorus is:

$$\frac{\delta}{\delta t} DOP = APC \bullet (BM \bullet B \bullet FPD + PR \bullet FPDP) + Klpop \bullet LPOP + Krpop \bullet RPOP - Kdop \bullet DOP \tag{32}$$

in which:

DOP = dissolved organic phosphorus (g P m^{-3})
LPOP = labile particulate organic phosphorus (g P m^{-3})
RPOP = refractory particulate organic phosphorus (g P m^{-3})
FPD = fraction of algal metabolism released as DOP ($0 < FPD < 1$)
FPDP = fraction of predation on algae released as DOP ($0 < FPDP < 1$)
Klpop = hydrolysis rate of LPOP (d^{-1})
Krpop = hydrolysis rate of RPOP (d^{-1})
Kdop = mineralization rate of DOP (d^{-1})

Labile Particulate Organic Phosphorus

The mass balance equation for labile particulate organic phosphorus is:

$$\frac{\delta}{\delta t} LPOP = APC \bullet (BM \bullet B \bullet FPL + PR \bullet FPLP) - Klpop \bullet LPOP - Wl \bullet \frac{\delta}{\delta z} LPOP \tag{33}$$

in which:

FPL = fraction of algal metabolism released as LPOP (0 < FPL < 1)
FPLP = fraction of predation on algae released as LPOP (0 < FPLP < 1)

Refractory Particulate Organic Phosphorus

The mass balance equation for refractory particulate organic phosphorus is:

$$\frac{\delta}{\delta t} RPOP = APC \bullet (BM \bullet B \bullet FPR + PR \bullet FPRP) - Krpop \bullet RPOP - Wr \bullet \frac{\delta}{\delta z} RPOP \quad (34)$$

in which:

FPR = fraction of algal metabolism released as RPOP (0 < FPR < 1)
FPRP = fraction of predation on algae released as RPOP (0 < FPRP < 1)

Nitrogen

The model nitrogen cycle (Figure 12) includes the following processes:

Algal production and metabolism
Predation
Hydrolysis of particulate organic nitrogen
Mineralization of dissolved organic nitrogen
Settling
Nitrification
Denitrification

External loads provide the ultimate source of nitrogen to the system. Available nitrogen is incorporated by algae during growth and released as ammonium+urea and organic nitrogen through respiration and predation. A portion of the particulate organic nitrogen hydrolyzes to dissolved organic nitrogen. The balance settles to the sediments. Dissolved organic nitrogen is mineralized to ammonium+urea. In an oxygenated water column, a fraction of the ammonium+urea is subsequently oxidized to nitrate+nitrite through the nitrification process. In anoxic water, nitrate+nitrite is lost to nitrogen gas through denitrification. Particulate nitrogen that settles to the sediments is mineralized and recycled to the water column, primarily as ammonium+urea. Nitrate+nitrite moves in both directions across the sediment-water interface, depending on relative concentrations in the water column and sediment interstices.

Nitrification

Nitrification is a process mediated by specialized groups of autotrophic bacteria that obtain energy through the oxidation of ammonium to nitrite and oxidation of nitrite to nitrate. A simplified expression for complete nitrification (Tchobanoglous and Schroeder 1987) is:

$$NH_4^+ + 2\,O_2 \rightarrow NO_3^- + H_2O + 2\,H^+ \qquad (35)$$

The simplified stoichiometry indicates that two moles of oxygen are required to nitrify one mole of ammonium into nitrate. The simplified equation is not strictly true, however. Cell synthesis by nitrifying bacteria is accomplished by the fixation of carbon dioxide so that less than two moles of oxygen are consumed per mole ammonium utilized (Wezernak and Gannon 1968).

The kinetics of complete nitrification are modeled as a function of available ammonium, dissolved oxygen, and temperature:

$$NT = \frac{DO}{KHont + DO} \bullet \frac{NH_4 - Urea}{KHnnt + NH_4 - Urea} \bullet f(T) \bullet NTm \qquad (36)$$

in which:

NT = nitrification rate (g N m^{-3} d^{-1})
KHont = half-saturation constant of dissolved oxygen required for nitrification (g O_2 m^{-3})
KHnnt = half-saturation constant of NH_4 required for nitrification (g N m^{-3})
NTm = maximum nitrification rate at optimal temperature (g N m^{-3} d^{-1})

The kinetics formulation (Figure 13) incorporates the products of two Monod-like functions. The first function diminishes nitrification at low dissolved oxygen concentration. The second function expresses the influence of ammonium concentration on nitrification. When ammonium concentration is low, relative to KHnnt, nitrification is proportional to ammonium concentration. For NH4 << KHnnt, the reaction is approximately first-order. (The first-order decay constant ≈ NTm/KHnnt.) When ammonium concentration is large, relative to KHnnt, nitrification approaches a maximum rate. This formulation is based on a concept proposed by Tuffey et al. (1974). Nitrifying bacteria adhere to benthic or suspended sediments. When ammonium is scarce, vacant surfaces suitable for nitrifying bacteria exist. As ammonium concentration increases, bacterial biomass increases, vacant surfaces are occupied, and the rate of nitrification increases. The bacterial population attains maximum density when all surfaces suitable for bacteria are occupied. At this point, nitrification proceeds at a maximum rate independent of additional increase in ammonium concentration.

The optimal temperature for nitrification may be less than peak temperatures that occur in coastal waters. To allow for a decrease in nitrification

at superoptimal temperature, the effect of temperature on nitrification is modeled in the Gaussian form of Equation 3.

Effect of Denitrification on Nitrate

The effect of denitrification on dissolved organic carbon has been described. Denitrification removes nitrate from the system in stoichiometric proportion to carbon removal:

$$\frac{\delta}{\delta t} NO_3 = -ANDC \bullet Denit \bullet DOC \tag{37}$$

in which:

ANDC = mass nitrate-nitrogen reduced per mass dissolved organic carbon oxidized (0.933 g N g^{-1} C)

Nitrogen Mass Balance Equations

The mass-balance equation for nitrogen state variables are written by summing all previously-described sources and sinks:

Ammonium+Urea

$$\frac{\delta}{\delta t} NH_4 - Urea - ANC \bullet \left[(BM \bullet FNI - PN \bullet P) \bullet B + PR \bullet FNIP\right] + Kdon \bullet DON - NT \tag{38}$$

in which:

FNI = fraction of algal metabolism released as NH4 ($0 \leq FNI \leq 1$)
PN = algal ammonium preference ($0 \leq PN \leq 1$)
FNIP = fraction of predation released as NH4 ($0 \leq FNIP \leq 1$)

Nitrate+Nitrite

$$\frac{\delta}{\delta t} NO_{23} = -ANC \bullet (1 - PN) \bullet P \bullet B + NT - ANDC \bullet Denit \bullet DOC \tag{39}$$

Dissolved Organic Nitrogen

$$\frac{\delta}{\delta t} DON = ANC \bullet (BM \bullet B \bullet FND + PR \bullet FNDP) + Klpon \bullet LPON + Krpon \bullet RPON - Kdon \bullet DON \tag{40}$$

in which:

DON = dissolved organic nitrogen (g N m^{-3})
LPON = labile particulate organic nitrogen (g N m^{-3})
RPON = refractory particulate organic nitrogen (g N m^{-3})
FND = fraction of algal metabolism released as DON (0 < FND < 1)
FNDP = fraction of predation on algae released as DON (0 < FNDP < 1)
Klpon = hydrolysis rate of LPON (d^{-1})
Krpon = hydrolysis rate of RPON (d^{-1})
Kdon = mineralization rate of DON (d^{-1})

Labile Particulate Organic Nitrogen

$$\frac{\delta}{\delta t} LPON = ANC \bullet (BM \bullet B \bullet FNL + PR \bullet FNLP) - Klpon \bullet LPON - Wl \bullet \frac{\delta}{\delta z} LPON \quad (41)$$

in which:

FNL = fraction of algal metabolism released as LPON (0 < FNL < 1)
FNLP = fraction of predation on algae released as LPON (0 < FNLP < 1)

Refractory Particulate Organic Nitrogen

$$\frac{\delta}{\delta t} RPON = ANC \bullet (BM \bullet B \bullet FPR + PR \bullet FPRN) - Krpon \bullet RPON - Wr \bullet \frac{\delta}{\delta z} RPON \quad (42)$$

in which:

FNR = fraction of algal metabolism released as RPON (0 < FNR < 1)
FNRP = fraction of predation on algae released as RPON (0 < FNRP < 1)

Silica

The model incorporates two siliceous state variables, dissolved silica and particulate biogenic silica. The silica cycle (Figure 14) is a simple one in which diatoms take up disolved silica and recycle dissolved and particulate biogenic silica through the actions of metabolism and predation. Particulate silica dissolves in the water column or settles to the bottom. A portion of the settled particulate biogenic dissolves within the sediments and returns to the water column as dissolved silica. Sources and sinks represented are:

Diatom production and metabolism

Predation
Dissolution of particulate to dissolved silica
Settling

Dissolved Silica

The kinetics equation for dissolved silica is:

$$\frac{\delta}{\delta t} Dsil = (FSAP \bullet PR - P) \bullet ASC \bullet B + Ksua \bullet PBS \qquad (43)$$

in which:

Dsil = dissolved silica (g Si m^{-3})
PBS = particulate biogenic silica concentration (g Si m^{-3})
FSAP = fraction of diatom silica made available by predation
$(0 \leq FSAP \leq 1)$
ASC = algal silica-to-carbon ratio (g Si g^{-1} C)
Ksua = particulate silica dissolution rate (d^{-1})

Particulate Biogenic Silica

The kinetics equation for particulate biogenic silica is:

$$\frac{\delta}{\delta t} PBS = \left(BM + (1 - FSAP) \bullet PR\right) \bullet ASC \bullet B - Wpbs \frac{\delta}{\delta z} PBS - Ksua \bullet PBS \qquad (44)$$

in which:

Wpbs = biogenic silica settling rate (m d^{-1})

An exponential function (Figure 4) describes the effect of temperature on silica dissolution.

Chemical Oxygen Demand

Chemical oxygen demand is the concentration of reduced substances that are oxidized through abiotic reactions. The source of chemical oxygen demand in saline water is sulfide released from sediments. A cycle occurs in which sulfate is reduced to sulfide in the sediments and reoxidized to sulfate in the water column. In freshwater, methane is released to the water column by the sediment model. Both sulfide and methane are quantified in units of oxygen demand and are treated with the same kinetics formulation:

$$\frac{\delta}{\delta t} COD = -\frac{DO}{KHocod + DO} \bullet Kcod \bullet COD$$

in which:

COD = chemical oxygen demand concentration (g oxygen-equivalents m^{-3})
KHocod = half-saturation concentration of dissolved oxygen required for exertion of chemical oxygen demand (g O_2 m^{-3})
Kcod = oxidation rate of chemical oxygen demand (d^{-1})

An exponential function (Figure 4) describes the effect of temperature on exertion of chemical oxygen demand.

Dissolved Oxygen

Sources and sinks of dissolved oxygen in the water column (Figure 15) include:

Algal photosynthesis
Atmospheric reaeration
Algal respiration
Heterotrophic respiration
Nitrification
Chemical oxygen demand

Reaeration

The rate of reaeration is proportional to the dissolved oxygen deficit in model segments that form the air-water interface:

$$\frac{\delta}{\delta t} DO = \frac{Kr}{\Delta z} \bullet (DOs - DO) \qquad (45)$$

in which:

DO = dissolved oxygen concentration (g O_2 m^{-3})
Kr = reaeration coefficient (m d^{-1})
DOs = dissolved oxygen saturation concentration (g O_2 m^{-3})
Δz = model layer thickness (m)

In freeflowing streams, the reaeration coefficient depends largely on turbulence generated by bottom shear stress (O'Connor and Dobbins 1958). In lakes and coastal waters, however, wind effects may dominate the reaeration process (O'Connor 1983). For Chesapeake Bay, a relationship for wind-driven gas exchange (Hartman and Hammond 1985) was employed:

$$Kr = Arear \bullet R\nu \bullet Wms^{1.5} \qquad (46)$$

in which:

Arear = empirical constant (≈0.1)
Rv = ratio of kinematic viscosity of pure water at 20 ^{o}C to kinematic viscosity of water at specified temperature and salinity
Wms = wind speed measured at 10 m above water surface (m s^{-1})

Hartman and Hammond (1985) indicate Arear takes the value 0.157. In the present model, Arear is treated as a variable to allow for effects of wind sheltering, for differences in height of local wind observations, and for other factors.

An empirical function (Figure 16) that fits tabulated values of Rv is:

$$Rv = 0.54 + 0.0233 \bullet T - 0.0020 \bullet S \tag{47}$$

in which:

S = salinity (ppt)
T = temperature (^{o}C)

Saturation dissolved oxygen concentration diminishes as temperature and salinity increase. An empirical formula that describes these effects (Genet et al. 1974) is:

$$\begin{aligned} DOs &= 14.5532 - 0.38217 \bullet T + 0.0054258 \bullet T^2 \\ &- CL \bullet (1.665 \times 10^{-4} - 5.866 \times 10^{-6} \bullet T + 9.796 \times 10^{-8} \bullet T^2) \end{aligned} \tag{48}$$

in which:

CL = chloride concentration (= salinity/1.80655)

Mass Balance Equation for Dissolved Oxygen

$$\begin{aligned} \frac{\delta}{\delta t} DO &= AOCR \bullet \left[(1.3 - 0.3 \bullet PN) \bullet P - (1 - FCD) \bullet BM \right] \bullet B \\ &- AONT \bullet NT - \frac{DO}{KHodoc + DO} \bullet AOCR \bullet Kdoc \bullet DOC \\ &- \frac{DO}{KHocod + DO} \bullet Kcod \bullet COD + \frac{Kr}{H} \bullet (DOs - DO) \end{aligned} \tag{49}$$

in which:

AOCR = oxygen-to-carbon mass ratio in production and respiration (= 2.67 g O_2 g^{-1} C)

AONT = oxygen consumed per mass ammonium nitrified (= 4.33 g O_2 g^{-1} N)

Temperature

Computation of temperature employs a conservation of internal energy equation that is analogous to the conservation of mass equation. For practical purposes, the internal energy equation can be written as a conservation of temperature equation. The only source or sink of temperature considered is exchange with the atmosphere. Atmospheric exchange is considered proportional to the temperature difference between the water surface and a theoretical equilibrium temperature (Edinger et al. 1974):

$$\frac{\delta}{\delta t}T = \frac{KT}{\rho \bullet Cp \bullet H} \bullet (Te - T) \tag{50}$$

in which:

T = water temperature (^oC)
Te = equilibrium temperature (^oC)
KT = Heat exchange coefficient (watt m^{-2} $^oC^{-1}$)
Cp = specific heat of water (4200 watt s kg^{-1} $^oC^{-1}$)
ρ = density of water (1000 kg m^{-3})

Inorganic (Fixed) Solids

The only kinetics transformation of fixed solids is settling:

$$\frac{\delta}{\delta t}ISS = -Wiss \bullet \frac{\delta}{\delta z}ISS \tag{51}$$

in which:

ISS = fixed solids concentration (g m^{-3})
Wiss = solids settling velocity (m d^{-1})

Salinity

Salinity is modeled by the conservation of mass equation with no internal sources or sinks

Parameter Values

Model parameter evaluation is a recursive process. Parameters are selected from a range of feasible values, tested in the model, and adjusted until satisfactory agreement between predicted and observed variables is obtained. Ideally, the range of feasible values is determined by observation or experiment.

For some parameters, however, no observations are available. Then, the feasible range is determined by parameter values employed in similar models or by the judgement of the modeler. A review of parameter values was included in documentation of the first application of this model (Cerco and Cole 1994). Parameters from the initial study were refined, where necessary, for the Virginia Tributary Refinements (Cerco et al. 2002) and refined again for the present model. A complete set of parameter values is provided in Table 2.

Table 1
Water Quality Model State Variables

Temperature	Salinity
Fixed Solids	Freshwater Group
Spring Diatoms	Other (Green) Algae
Microzooplankton	Mesozooplankton
Dissolved Organic Carbon	Labile Particulate Organic Carbon
Refractory Particulate Organic Carbon	Ammonium+Urea
Nitrate+Nitrite	Dissolved Organic Nitrogen
Labile Particulate Organic Nitrogen	Refractory Particulate Organic Nitrogen
Total Phosphate	Dissolved Organic Phosphorus
Labile Particulate Organic Phosphorus	Refractory Particulate Organic Phosphorus
Chemical Oxygen Demand	Dissolved Oxygen
Dissolved Silica	Particulate Biogenic Silica

Table 2
Parameters in Kinetics Equations

Symbol	Definition	Value	Units
AANOX	ratio of anoxic to oxic respiration	0.5	$0 \leq AANOX \leq 1$
ANC	nitrogen-to-carbon ratio of algae	0.135 (spring), 0.175 (other)	g N g^{-1} C
AOCR	dissolved oxygen-to-carbon ratio in respiration	2.67	g O_2 g^{-1} C
AONT	mass dissolved oxygen consumed per mass ammonium nitrified	4.33	g O_2 g^{-1} N
APC	algal phosphorus-to-carbon ratio	0.0175 (green), 0.0125 (other)	g P g^{-1} C
Areaer	empirical constant in reaeration equation	0.078	
ASC	algal silica-to-carbon ratio	0.4 (Group 1), 0.4 (spring), 0.3 (green)	g Si g^{-1} C
BM	basal metabolic rate of algae at reference temperature Tr	0.03 (Group 1), 0.01 (spring), 0.02 (green)	d^{-1}
CChl	carbon-to-chlorophyll ratio	30 (Group 1), 90 (spring), 50 (green)	g C g^{-1} Chl
FCD	fraction of dissolved organic carbon produced by algal metabolism	0.0	$0 \leq FCD \leq 1$
FCDP	fraction of dissolved organic carbon produced by predation	0.15	$0 \leq FCDP \leq 1$
FCL	fraction of labile particulate carbon produced by algal metabolism	0.0	$0 \leq FCL \leq 1$
FCLP	fraction of labile particulate carbon produced by predation	0.65	$0 \leq FCLP \leq 1$
FCR	fraction of refractory particulate carbon produced by algal metabolism	0.0	$0 \leq FCR \leq 1$
FCRP	fraction of refractory particulate carbon produced by predation	0.2	$0 \leq FCRP \leq 1$
FNI	fraction of inorganic nitrogen produced by algal metabolism	0.55	$0 \leq FNI \leq 1$
FNIP	fraction of inorganic nitrogen produced by predation	0.4	$0 \leq FNIP \leq 1$
FND	fraction of dissolved organic nitrogen produced by algal metabolism	0.2	$0 \leq FND \leq 1$
FNDP	fraction of dissolved organic nitrogen	0.2	$0 \leq FNDP \leq 1$

Table 2
Parameters in Kinetics Equations

Symbol	Definition	Value	Units
	produced by predation		
FNL	fraction of labile particulate nitrogen produced by algal metabolism	0.2	$0 \leq FNL \leq 1$
FNLP	fraction of labile particulate nitrogen produced by predation	0.25	$0 \leq FNLP \leq 1$
FNR	fraction of refractory particulate nitrogen produced by algal metabolism	0.05	$0 \leq FNR \leq 1$
FNRP	fraction of refractory particulate nitrogen produced by predation	0.15	$0 \leq FNRP \leq 1$
FPD	fraction of dissolved organic phosphorus produced by algal metabolism	0.25	$0 \leq FPD \leq 1$
FPDP	fraction of dissolved organic phosphorus produced by predation	0.4	$0 \leq FPDP \leq 1$
FPI	fraction of dissolved inorganic phosphorus produced by algal metabolism	0.5	$0 \leq FPI \leq 1$
FPIP	fraction of dissolved inorganic phosphorus produced by predation	0.75	$0 \leq FPIP \leq 1$
FPL	fraction of labile particulate phosphorus produced by algal metabolism	0.0	$0 \leq FPL \leq 1$
FPLP	fraction of labile particulate phosphorus produced by predation	0.07	$0 \leq FPLP \leq 1$
FPR	fraction of refractory particulate phosphorus produced by algal metabolism	0.0	$0 \leq FPR \leq 1$
FPRP	fraction of refractory particulate phosphorus produced by predation	0.03	$0 \leq FPRP \leq 1$
FSAP	fraction of dissolved silica produced by predation	0.5	$0 \leq FSAP \leq 1$
Kcod	oxidation rate of chemical oxygen demand	20	d^{-1}
Kdoc	dissolved organic carbon respiration rate	0.011 to 0.075	d^{-1}
Kdon	dissolved organic nitrogen mineralization rate	0.025	d^{-1}
Kdp	minimum mineralization rate of dissolved organic phosphorus	0.15	d^{-1}
Kdpalg	constant that relates mineralization rate to algal biomass	0.4	$m^3\ g^{-1}\ C\ d^{-1}$
KHn	half-saturation concentration for nitrogen uptake by algae	0.02 (Group 1), 0.025 (other)	$g\ N\ m^{-3}$
KHndn	half-saturation concentration of nitrate required for denitrification	0.1	$g\ N\ m^{-3}$
KHnnt	half-saturation concentration of NH_4 required	1.0	$g\ N\ m^{-3}$

Table 2
Parameters in Kinetics Equations

Symbol	Definition	Value	Units
	for nitrification		
KHocod	half-saturation concentration of dissolved oxygen required for exertion of COD	0.5	g O_2 m^{-3}
KHodoc	half-saturation concentration of dissolved oxygen required for oxic respiration	0.5	g O_2 m^{-3}
KHont	half-saturation concentration of dissolved oxygen required for nitrification	1.0	g O_2 m^{-3}
KHp	half-saturation concentration for phosphorus uptake by algae	0.0025	g P m^{-3}
KHs	half-saturation concentration for silica uptake by algae	0.01 (Group 1), 0.03 (spring), 0.01 (green)	g Si m^{-3}
KHst	salinity at which algal mortality is half maximum value	2.0 (Group 1), 2.0 (spring)	ppt
Klpoc	labile particulate organic carbon dissolution rate	0.02 to 0.15	d^{-1}
Klpon	labile particulate organic nitrogen hydrolysis rate	0.12	d^{-1}
Klpop	labile particulate organic phosphorus hydrolysis rate	0.24	d^{-1}
Krpoc	refractory particulate organic carbon dissolution rate	0.005 to 0.01	d^{-1}
Krpon	refractory particulate organic nitrogen hydrolysis rate	0.005	d^{-1}
Krpop	refractory particulate organic phosphorus hydrolysis rate	0.01	d^{-1}
Ksua	biogenic silica dissolution rate	0.1	d^{-1}
KTb	effect of temperature on basal metabolism of algae	0.032	$^oC^{-1}$
KTcod	effect of temperature on exertion of chemical oxygen demand	0.041	d^{-1}
KTg1	effect of temperature below Tm on growth of algae	0.008 (Group 1), 0.0018 (spring), 0.0035 (green)	$^oC^{-2}$
KTg2	effect of temperature above Tm on growth of algae	0.004 (Group 1), 0.006 (spring), 0.0 (green)	$^oC^{-2}$
KThdr	effect of temperature on hydrolysis rates	0.032	$^oC^{-1}$
KTmnl	effect of temperature on mineralization rates	0.032	$^oC^{-1}$
KTnt1	effect of temperature below Tmnt on	0.003	$^oC^{-2}$

Table 2
Parameters in Kinetics Equations

Symbol	Definition	Value	Units
	nitrification		
KTnt2	effect of temperature above Tmnt on nitrification	0.003	$^oC^{-2}$
KTsua	effect of temperature on biogenic silica dissolution	0.092	$^oC^{-1}$
NTm	maximum nitrification rate at optimal temperature	0.1 to 0.5	g N m^{-3} d^{-1}
Phtl	predation rate on algae	0.1 (Group 1), 0.1 to 0.2 (spring), 0.5 to 2 (green)	m^3 g^{-1} C d^{-1}
Pm^B	maximum photosynthetic rate	270 (Group 1), 300 (spring), 350 (green)	g C g^{-1} Chl d^{-1}
Presp	photo-respiration fraction	0.25	$0 \leq Presp \leq 1$
STF	salinity toxicity factor	0.3 (Group 1), 0.1 (spring)	d^{-1}
Topt	optimal temperature for growth of algae	29 (Group 1), 16 (spring), 25 (green)	^oC
Tmnt	optimal temperature for nitrification	30	^oC
Tr	reference temperature for metabolism	20	^oC
Trhdr	reference temperature for hydrolysis	20	^oC
Trmnl	reference temperature for mineralization	20	^oC
Trsua	reference temperature for biogenic silica dissolution	20	^oC
Wa	algal settling rate	0.1 (Group 1), 0.1 (other)	m d^{-1}
Wl	settling velocity of labile particles	0.1	m d^{-1}
Wr	settling velocity of refractory particles	0.1	m d^{-1}
Wiss	settling velocity of fixed solids	1 to 4	m d^{-1}
Wpbs	settling velocity of biogenic silica	0.1	m d^{-1}
α	initial slope of production vs. irradiance relationship	3.15 (Group 1), 8.0 (other)	g C g^{-1} Chl $(E\ m^{-2})^{-1}$

References

Ammerman, J., and Azam, F. (1985). "Bacterial 5'-nucleodase in aquatic ecosystems: a novel mechanism of phosphorus regeneration," *Science,* 227, 1338-1340.

Boni, L., Carpene, E., Wynne, D., and Reti, M. (1989). "Alkaline phosphatase activity in *Protogonyaulax Tamarensis*," *Journal of plankton research,* 11, 879-885.

Bunch, B., Cerco, C., Dortch, M., Johnson, B., and Kim, K. (2000). "Hydrodynamic and water quality model study of San Juan Bay and Estuary," ERDC TR-00-1, U.S. Army Engineer Research and Development Center, Vicksburg MS.

Cerco, C., and Cole, T. (1994). "Three-dimensional eutrophication model of Chesapeake Bay," Technical Report EL-94-4, US Army Engineer Waterways Experiment Station, Vicksburg, MS.

Cerco, C., Bunch, B., Cialone, M., and Wang, H. (1994). "Hydrodynamic and eutrophication model study of Indian River and Rehoboth Bay, Delaware," Technical Report EL-94-5, US Army Engineer Waterways Experiment Station, Vicksburg, MS.

Cerco, C., and Bunch, B. (1997). "Passaic River tunnel diversion model study, Report 5, water quality modeling," Technical Report HL-96-2, US Army Engineer Waterways Experiment Station, Vicksburg, MS.

Cerco, C., Johnson, B., and Wang, H. (2002). "Tributary refinements to the Chesapeake Bay model," ERDC TR-02-4, US Army Engineer Research and Development Center, Vicksburg, MS.

Cerco, C. and Noel, M. (2003). " The 2002 Chesapeake Bay euptrophication model." ERDC TR-03-XX, US Army Engineer Research and Development Center, Vicksburg, MS

Chrost, R., and Overbeck, J. (1987). "Kinetics of alkaline phosphatase activity and phosphorus availability for phytoplankton and bacterioplankton in Lake Plubsee (north German eutrophic lake)," *Microbial Ecology,* 13, 229-248.

Edinger, J., Brady, D., and Geyer, J. (1974). "Heat exchange and transport in the environment," Report 14, Department of Geography and Environmental Engineering, Johns Hopkins University, Baltimore, MD.

Genet, L., Smith, D., and Sonnen, M. (1974). "Computer program documentation for the Dynamic Estuary Model," US Environmental Protection Agency, Systems Development Branch, Washington, DC.

Hartman, B., and Hammond, D. (1985). "Gas exchange in San Francisco Bay," *Hydrobiologia* 129, 59-68.

HydroQual (2000). "Development of a suspension feeding and deposit feeding benthos model for Chesapeake Bay," Project USCE0410, prepared for US Army Engineer Research and Development Center, Vicksburg MS.

Jassby, A., and Platt, T. (1976). "Mathematical formulation of the relationship between photosynthesis and light for phytoplankton," *Limnology and Oceanography* 21, 540-547.

Leonard, B. (1979). "A stable and accurate convection modelling procedure based on quadratic upstream interpolation," *Computer Methods in Applied Mechanics and Engineering,* 19, 59-98.

Matavulj, M., and Flint, K. (1987). "A model for acid and alkaline phosphatase activity in a small pond," *Microbial Ecology,* 13, 141-158.

Monod, J. (1949). "The growth of bacterial cultures," *Annual Review of Microbiology* 3, 371-394.

Morel, F. (1983). *Principles of Aquatic Chemistry,* John Wiley and Sons, New York, NY, 150.

O'Connor, D., and Dobbins, W. (1958). "Mechanisms of reaeration in natural streams," *Transactions of the American Society of Civil Engineers,* 123, 641-666.

O'Connor, D. (1983). "Wind effects on gas-liquid transfer coefficients," *Journal of the Environmental Engineering Division,* 190, 731-752.

Parsons, T., Takahashi, M., and Hargrave, B. (1984). *Biological oceanographic processes*. 3rd ed., Pergamon Press, Oxford.

Stumm, W., and Morgan, J. (1981). *Aquatic chemistry.* 2nd ed., Wiley-Interscience, New York.

Thomann, R., and Fitzpatrick, J. (1982). "Calibration and verification of a mathematical model of the eutrophication of the Potomac Estuary," HydroQual Inc., Mahwah, NJ.

Tchobanoglous, G., and Schroeder, E. (1987). *Water quality,* Addison Wesley, Reading, MA.

Tuffey, T., Hunter, J., and Matulewich, V. (1974). "Zones of nitrification", *Water Resources Bulletin*, 10, 555-564.

Wezernak, C., and Gannon, J. (1968). "Evaluation of nitrification in streams,"

Journal of the Sanitary Engineering Division, 94(SA5), 883-895.

6 Water Quality Model Results

We have completed a model that provides a first-order representation of eutrophication processes in the Chester system including the Chester River and the Eastern Bay. Time series plots at the CBP long-term station in the system showed reasonable behavior of water quality variables (Appendix 5-A). The model was not able to capture high concentration of bottom chlorophyll during spring at the entrance of the Eastern Bay (EE1.1) and the Chester River (ET4.2). This is also shown for the main Bay. At the upstream station of the Chester River (ET4.1) Dissolved Oxygen was higher in the model during summer, especially in 1998. The influence of the main Bay appears only substantial near the mouths (EE1.1 and ET4.2). The cumulative distribution plots (Appendix 5-B) show reasonable bottom Dissolved Oxygen prediction at EE1.1 and ET4.2 and surface Chlorophyll prediction at ET4.1. The cumulative distribution plots for the 1999 MDE intensive survey stations in the Chester River (Appendix 5-C) show reasonable bottom Dissolved Oxygen prediction. In the Eastern Bay and its tributaries, including Miles, Wye, and Wye East Rivers, show reasonable Dissolved Oxygen prediction but Chlorohpyll prediction was off. This suggests that the Dissolved Oxygen, influenced by the conditions of the main Bay that is considered well simulated. It is suspected, however, that the loading from the adjacent watersheds for the Eastern Bay tributaries were not adequate. This was also shown by the salinity simulation of hydrodynamic model. We compared longitudinal distribution during wet (Appendix 5-E) and dry (Appendix 5-F) seasons over the 1999 MDE intensive survey stations. The prediction followed the similar spatial distribution patterns to the observation. Ammonium around 40 km shows abnormality. This is where Morgan Creek flows into the Chester River. The predicted sediment flux also was close to that of observation (Appendix 5-G).

Figure Captions

Appendix 5-A

This appendix contains time series plots of observed and computed properties (surface and bottom) at CBP long term stations EE1.1, ET4.1, and ET4.2.

Appendix 5-B

This appendix contains cumulative distribution plots of observed and computed properties (surface and bottom) at CBP long term stations EE1.1, ET4.1, and ET4.2.

Appendix 5-C

This appendix contains cumulative distribution plots of observed and computed properties (surface and bottom) at 1999 MDE intensive survey stations in the Chester River.

Appendix 5-D

This appendix contains cumulative distribution plots of observed and computed properties (surface and bottom) at 1999 MDE intensive survey stations in the Eastern Bay and its tributaries, including, Miles, Wye, and Wye East Rivers.

Appendix 5-E

This appendix contains longitudinal plots of computed and observed properties at 1999 MDE intensive survey stations in the Chester River during wet season (March – May).

Appendix 5-F

This appendix contains longitudinal plots of computed and observed properties at 1999 MDE intensive survey stations in the Chester River during dry season (June – August).

Appendix 5-G

This appendix compares time series plots of observed and computed sediment oxygen and nutrient exchange. Data from 2000 is grouped by month and compared to model results from 1997-1999.